Geochemical investigation of the taphonomy, stratigraphy, and palaeoecology of the mammals from the Ouled Abdoun Basin (Paleocene-Eocene of Morocco)

László Kocsis, Alex Ulianov, Mustapha Mouflih, Fatima Khaldoune, Emmanuel Gheerbrant

Geochemical investigation of the taphonomy, stratigraphy, and palaeoecology of the mammals from the Ouled Abdoun Basin (Paleocene-Eocene of Morocco)

László Kocsis[1,*], Alex Ulianov[2], Mustapha Mouflih[3], Fatima Khaldoune[4], Emmanuel Gheerbrant[5]

[1]Geology Group, Universiti Brunei Darussalam (UBD), Brunei Darussalam, email: laszlokocsis@hotmail.com

[2]Institute of Earth Sciences, University of Lausanne, Switzerland, email: alexey.ulyanov@unil.ch

[3]Hassan II University of Casablanca, Sedimentary Basins Dynamic and Geological Correlations Lab, Casablanca, Morocco, email: moufli@yahoo.fr

[4]Groupe Office Chérifien des Phosphates, Centre Minier de Khouribga, Morocco, email: khaldoune.fatima@ocpgroup.ma

[5]CR2P, Sorbonne Université, CNRS-MNHN-UPMC, Paris, France, email: emmanuel.gheerbrant@mnhn.fr

*corresponding author: laszlokocsis@hotmail.com, laszlo.kocsis@ubd.edu.bn

ABSTRACT

We performed different geochemical analyses of Paleogene terrestrial mammal remains to establish their taphonomy, stratigraphic provenance, and palaeoenvironmental conditions. Rare earth element (REE) results indicate a similar diagenetic history to that of previously investigated marine taxa from these beds. Therefore, the mammal remains were initially deposited in a marine setting, and probably not long after the death of the animals their bodies were washed into the sea. The Ce/Ce* and Pr/Pr* ratios for the mammal fossils were compared with the background dataset from the phosphate mines, which varies with time. This allowed us to characterize the stratigraphic levels bearing the fossils. The provenances of fossils with known origins were confirmed, while remains with unknown origins could be assigned to certain stratigraphic horizons that are compatible with previously proposed phylogenic relationships.

Marine diagenesis affected the various skeletal tissues differently, with the largest alteration in the bone and the least or none in the enamel. This is mostly demonstrated by the high F concentration, high Ca/P, and seawater related $^{87}Sr/^{86}Sr$ in the bone/dentine samples. Enamel shows the opposite, and retained the most pristine terrestrial values. The $\delta^{18}O_{PO4}$ and $\delta^{13}C$ results from mammal enamel revealed warm (>20°C mean annual temperature-MAT) and dry (<500mm mean annual precipitation) conditions for Paleocene-Eocene period in the region. From the early to mid-Ypresian about +5°C ΔMAT is recorded that might be linked to the Early Eocene Climatic Optimum.

Furthermore, the $^{87}Sr/^{86}Sr$ ratios derived from shark tooth enameloid fit the global open ocean Sr-isotope record during the latest Paleocene and early Eocene providing further evidence for the age of these phosphate beds in the Ouled Abdoun Basin. However, older marine fossils yielded higher ratios than the global Sr-isotope curve, reflecting an alteration and/or somewhat restricted conditions in the Moroccan coastal basins, possibly triggered by global sea-level changes.

Keywords: bioapatite, rare earth elements, stable isotopes, strontium isotopes, phosphorite.

1. Introduction

The phosphate series of the Ouled Abdoun Basin in Morocco, which is exploited in large industrial quarries, is renowned for its Upper Cretaceous-Lower Eocene vertebrate assemblages (e.g., Arambourg, 1952; Bardet et al., 2017). The fauna predominantly comprises sub-autochthonous marine aquatic organisms such as cartilaginous and bony fishes, mosasaurs, and turtles, but occasionally terrestrial remains have also been described, such as non-avian dinosaurs, birds, and mammals (e.g., Gheerbrant et al., 2003; Pereda Suberbiola et al., 2004; Bourdon et al., 2005). The mammals are rare and most of the time scientists come to know about them from private collectors living near the phosphate quarries, and often cannot determine their precise stratigraphic origin. Knowing the stratigraphic origins of the Ouled Abdoun fossils is crucial to elucidating the early Cenozoic evolution of African mammals (e.g., Gheerbrant et al., 2018). Accurate dating of the Ouled Abdoun mammals is also important for knowledge and characterization of the early Cenozoic successive African faunal assemblages.

To tackle the stratigraphic origins of vertebrate remains, geochemical taphonomy is a widely used method (e.g., Staron et al., 2001; Trueman et al., 2003; Metzger et al., 2004; MacFadden et al., 2007; Suarez et al., 2010; Herwartz et al., 2013; Botfalvai et al., 2021). This is based on trace element contents that are absent or occur only in very low concentrations (sub-ppm) in modern bones and teeth, however, after the death of the animals their concentrations increase through the influence of the sedimentary environment (e.g., Elderfield and Pagett, 1986). The most widely used elements are the rare earths (REE) and uranium, which can reach 4-5 orders of magnitude enrichment in fossil material compared to modern concentrations (e.g., Trueman and Tuross, 2003). These elements therefore could reflect the chemistry of the pore fluid in which the vertebrate remains were fossilized. There are several studies using REE chemistry of fossil bioapatite to reconstruct palaeoenvironmental conditions in terrestrial and marine depositional settings (e.g., Trueman et al., 2003; Lécuyer et al. 2004; Shield and Webb, 2004; Kocsis et al., 2009; Žigaitė et al., 2016; 2020), which are all based on the assumption that REEs are quantitatively taken up from the burial environment (e.g., Reynard et al., 1999). During their incorporation into the bioapatite structure, however, fractionation could occur between the light and heavy REEs due to size differences along the REE series and related diffusion (e.g., Trueman et al., 2011; Herwartz et al., 2013). In addition, protracted late diagenetic modification (Kocsis et al., 2010; Herwartz et al., 2011) may further complicate environmental interpretations, especially for older samples (Kowal-Linka et al., 2014). To address these issues, a large number of samples, including different types of materials (e.g., bones, teeth, enamel, and dentine), and multiple *in-situ* analyses, are needed to evaluate further the origin of the REEs within the bioapatite.

In relation to the Moroccan phosphate series in the Ouled Abdoun and Ganntour basins, the trace element chemistry of nearly 200 marine samples (fish teeth, bones, coprolites) was published in Kocsis et al. (2016). Fractionation and late diagenetic overprint were completely ruled out. All the samples yielded similar, typical oxic seawater REE distributions with heavy REE enrichment and a negative Ce-anomaly. Importantly, however, the Ce-anomalies show a distinct change with stratigraphic level (Kocsis et al., 2016), a trend that is used in this work to assign a stratigraphic age for unprovenanced fossils. Such an approach was successful for the Embrithopoda mammal taxa of *Stylolophus minor* and *S. major* in the Ouled Abdoun Basin (Gheerbrant et al., 2018).

The main aim of this study is to further investigate the validity of the trace element provenancing method for the rare mammal fossils with known and unknown origins in the Ouled Abdoun Basin. To help better assess the taphonomy of these remains, major and other trace elements, and strontium isotope ratios ($^{87}Sr/^{86}Sr$) of selected mammal fossils, were compared with marine end-members such as data from shark teeth. Enameloid $^{87}Sr/^{86}Sr$ data derived from the latter also provide a proxy for the age of the phosphate beds, through comparing their ratios with the global $^{87}Sr/^{86}Sr$ record. In addition, some mammal fossils were measured for their stable oxygen and carbon isotopic compositions to get an insight into the ecological conditions of some of these early African placental mammals.

2. Geological and stratigraphical settings

The Ouled Abdoun Basin is one of the ancient epicontinental marine basins along the Atlantic coast of Africa, where large amounts of phosphorite accumulated during the late Cretaceous - early Eocene period. The basement rocks are covered by Cenomanian-Turonian carbonates followed by yellow marls with possible age within the Coniacian-Campanian interval (El Assel et al., 2013), which were eventually succeeded by the phosphorite series. The top of the succession is either covered by Lutetian dolomitic limestone or by Neogene continental beds (OCP, 1989). In the phosphorite series, three sequences (A-C) of 2nd order transgressive-regressive (T-R) cycles (Vail et al., 1991) are recognized, with ages of Maastrichtian (latest Cretaceous) (A), Danian-Thanetian (Paleocene) (B), and Ypresian (early Eocene) (C). These T-R cycles are further divided into 3rd order cycles that begin with P-rich phosphate (often granular in appearance), and end with clayey, carbonate, or siliceous deposits. The phosphorite series is often followed by a fourth sequence (D) but without phosphate occurrences (EL Haddi, 2014), marking the reduction of phosphogenesis and the installation of silicified limestone with lumachellic texture and the occurrence of Thersitea-type gastropods (Mouflih, 2015).

Regional correlation and biostratigraphy of these sediments are achieved by examining selachian remains (i.e., shark and ray teeth), which are extremely abundant (e.g., Arambourg, 1952; Noubhani and Cappetta, 1997; Cappetta et al., 2014), while other, non-phosphatic fossils are either very poorly preserved or do not have significant stratigraphic value (e.g., Ollivier-Pierre, 1982; Rauscher, 1985; Soncini, 1990). Chemostratigraphy based

on the $\delta^{13}C$ of residual organic matter (Yans et al., 2014) and the $\delta^{18}O$ and $\delta^{13}C$ of marine vertebrate fossils (Kocsis et al., 2014a), however, revealed some details about the timing of the Paleogene beds such as (1) sedimentation occurred during the middle Paleocene (Selandian, 61.5-59.2 Ma); (2) a possible lack of sedimentation during the latest Paleocene (late Thanetian, ~57-56 Ma), probably including the Paleocene-Eocene Thermal Maximum (PETM); and (3) the third sequence (C) was deposited during the early Eocene (early - ?late Ypresian, ~56-51 Ma) including the Early Eocene Climatic Optimum (EECO).

Traditionally, the phosphate succession in the Ouled Abdoun Basin is further subdivided into several phosphate-rich beds of industrial value (from base to top, beds III, II, I, 0) with the non-exploited horizons of calcareous phosphate, chert, or thin clay between them called intercalary beds (Figure 1). Bed III refers to the Late Cretaceous layers, Bed IIa and Bed IIb to the Paleocene beds, while Bed I, Bed 0', Bed 0, and the top layers called "sillons" are early Eocene, as determined from the associated selachian faunas (Arambourg, 1952; Noubhani and Cappetta, 1997) (Figure 1). Upsection the proportions of phosphate decrease and chert-rich sediments occur more often. The successive phosphate beds recurrently enclose "bone beds" where vertebrate remains are concentrated, probably as a result of hydrodynamic accumulations and/or during a period of condensation of bioclastic material with a low sedimentation rate (Gheerbrant et al., 2003). Three of them also yielded unique mammal remains: (1) the *Eritherium* bone bed at the base of Bed IIa, dated Selandian (61.6 - 59.2 Ma); (2) the big coprolite bone bed in the upper part of Bed IIa, dated Thanetian (59.2-56 Ma); and (3) the earliest Ypresian (~56-55 Ma) *Otodus obliquus* bone bed within intercalary bed II/I (Figure 1). Mammals also derived from two younger levels (Figure 1) such as (4) the base of Bed I, dated lower Ypresian (~55-54 Ma); and (5) the upper phosphate horizons, Bed 0 and the "sillons", dated middle Ypresian (~53-51 Ma) (Yans et al., 2014; Kocsis et al., 2014a).

The mammals recovered from these Paleocene and lower Eocene phosphate beds are the earliest known placentals in Africa, together with those from the Ouarzazate Basin (Gheerbrant et al., 2017). Despite their rarity, they document an unexpected taxonomic diversity, especially for paenungulates (Afrotheria), which comprise 7 genera and 10 species (*Abounodus*, *Ocepeia daouiensis*, *O. grandis*, *Eritherium*, *Phosphatherium*, *Daouitherium*, *Seggeurius*, Paenungulata indet., *Stylolophus minor,* S. *major*; see Gheerbrant et al., 1998, 2001, 2003, 2009, 2014, 2018; Bardet et al., 2017).

3. Material and Methods

3.1. Investigated materials

Several mammal species and/or other fossils from the mammal-related sediment matrix were involved in our research. Some of the fossils have known stratigraphic positions, while the origins of the others are questionable or completely unknown (Table 1). We focused primarily on the trace element compositions of the fossils (Table 1). However, some specimens were also analyzed for the presence of major elements (Ca, P, F), stable oxygen and carbon isotopes, and radiogenic strontium isotopes. The latter taxa are *Daouitherium rebouli* (Bed 0), *Phosphatherium escuilliei* (intercalary Bed II/Bed I, and Bed I), Hyracoidea indet (unknown bed; Gheerbrant et al., 2003), *Ocepeia grandis* (Bed IIa; Gheerbrant et al., 2014), and *Eritherium azzouzorum* (base of Bed IIa, i.e., *Eritherium* bone bed). These mammals are mostly known by fragments of jaws and, in the best cases, by a few skulls, and all of them are early representatives of the African endemic placental ungulates (Paenungulata). In particular *Eritherium* (Gheerbrant, 2009, Gheerbrant et al., 2012), *Phosphatherium* (Gheerbrant et al., 2005), and *Daouitherium* (Gheerbrant et al., 2002) are the earliest and most basal proboscideans. They document the very early emergence in Africa of one of the most remarkable lineage of extant placentals, the elephant order (Gheerbrant, 2009).

Often different parts have been analyzed and compared in parallel, such as mammal tooth enamel and dentine, bone, and – from the sediment matrix – shark tooth enameloid, dentine, and coprolites. More details about the analyses of these are presented in the Methods section.

In addition, the background trace element dataset (Kocsis et al., 2016) is extended here by samples analyzed from the big coprolite bone bed (upper part of Bed IIa) from quarries of Sidi Chennane (N32°38'25'', W6°43'22'') and Sidi Daoui (Meraa El Arech Nord - N32°46'47'', W6°45'4''), while a few specimens from the *Eritherium* and *Otodus obliquus* bone beds were also added from Sidi Daoui near Meraa El Arech Nord and Boujniba (N32°52'16'', W6°47'13''), respectively (Supplementary Material Table-1).

3.2. Major and trace element compositions

All the analyses were carried out at the Institute of Earth Sciences, University of Lausanne, Switzerland. The mammal remains (teeth and bones) and fossils from the associated matrix (fish teeth, coprolites) were cut with a micro-saw, then small pieces were embedded in epoxy resin and flat-polished. The major-element contents of selected fossils were determined by using wavelength-dispersive analysis with a JEOL 8200 microprobe. The concentrations of rare earth and other trace elements were measured by Laser Ablation-Inductively Coupled Plasma-Mass Spectrometry (LA-ICP-MS), using a GeoLas 200M ArF excimer laser (193nm) coupled to a Perkin-Elmer ELAN 6100 DRC quadrupole spectrometer or via Element XR ICP-MS with a linked RESOlution ablation system. The ablation was carried out in a He atmosphere using spot sizes of 60-80 µm in diameter. Standard reference materials 612 from NIST, representing silica-lime-alumina glasses doped with trace elements, were used for external standardization (Pearce et al., 1997). ^{42}Ca was analyzed as an internal standard; CaO values of 54, 51 and 50 wt.% were used respectively for shark tooth enameloid, mammal enamel, and for more porous material such as dentine, bone and coprolites. These values are the overall average CaO content of the different remains derived from the microprobe data presented here (Supplementary Material Table-2) and provided in Kocsis et al. (2014a). The analytical reproducibility was generally better than ±5% SE.

3.3. Strontium isotope ratios ($^{87}Sr/^{86}Sr$)

The chemical separation of Sr and mass spectrometry were performed at the Department of Earth Sciences, University of Geneva (Switzerland). Selected fossils were cleaned in an ultrasonic bath to reduce any sedimentary contamination, then the external 0.5-1 mm surface was removed that might have been altered in the depositional environment. From the cleaned surface about 2-5 mg of mammal enamel(oid) / dentine / bone powder was obtained using a micro-drill, and was dissolved in Teflon beakers at 80°C in 2M HCl. Sr separation was performed by extraction chromatography using Eichrom's Sr-Spec resin according to a protocol modified from Pin et al. (1994). Strontium was analysed in 2% HNO_3 solution on a Neptune Plus Multi Collector ICP-MS. Interferences at masses ^{84}Sr (^{84}Kr), ^{86}Sr (^{86}Kr) and ^{87}Sr (^{87}Rb) were corrected by monitoring ^{83}Kr and ^{85}Rb. Mass fractionation was internally corrected assuming a $^{88}Sr/^{86}Sr$ ratio of 8.375209. The values were internally corrected further for external fractionation based on repeat analyses of the

strontium NBS 987 standard (nominal value of 0.710248), which yielded an average $^{87}Sr/^{86}Sr$ value of 0.710270 (10 ppm long-term reproducibility, 1σ).

3.4. Stable isotope analyses ($\delta^{18}O_{PO4}$, $\delta^{13}C$, $\delta^{18}O_{CO3}$)

The sample preparation and analyses were performed in the Stable Isotope Laboratory of the Institute of Earth Surface Dynamics at the University of Lausanne, Switzerland. Sample preparation and some of the analytical backgrounds are summarized in Kocsis et al. (2014a). The oxygen isotope composition of PO_4^{3-} ion was analysed with a high-temperature conversion elemental analyser (TC/EA) coupled to a Finnigan MAT Delta Plus XL mass spectrometer. The results were corrected to in-house Ag_3PO_4 phosphate standards (LK-2 L: 12.1‰ and LK-3 L: 17.9‰) with better than ±0.3‰ (1σ) standard deviations during the runs. NBS-120c phosphorite reference material was prepared in parallel with the samples and an average value of 21.6 ± 0.3‰ (n = 10) was obtained. The carbon and oxygen isotope compositions of the structural carbonate in the apatite were analysed with a Gasbench II coupled to a Finnigan MAT Delta Plus XL mass spectrometer. The measured isotopic ratios were normalized to an in-house Carrara marble calcite standard that is calibrated against NBS-19. The analytical precision for this method is better than ±0.1‰ for O and C isotopes. The data are expressed in delta notation, in the case of $\delta^{18}O_{PO4}$ relative to VSMOW (Vienna Standard Mean Ocean Water), while the $\delta^{13}C$ and $\delta^{18}O_{CO3}$ results from the structural carbonate analyses are shown relative to VPDB (Vienna Pee Dee Belemnite).

4. Results

4.1. Major element compositions

The remains of four mammal taxa, *Daouitherium rebouli* (PM65), *Phosphatherium escuilliei* (MNHN.F PM25), Hyracoidea indet (MNHN.F PM52), and *Ocepeia grandis* (PM66) were analyzed for CaO, P_2O_5 and F content (Table 2, Figure 2). The Ca/P ratio ranges from 1.70 to 2.02, with the values increasing from enamel to dentine to bone. The F content varies between 0.73 and 3.95 wt% and a similar trend to the Ca/P ratio can be seen, as the lower values come from the enamel, and the highest ones from the bone samples (Figure 2).

4.2. Trace element compositions

Nineteen mammal specimens, sometimes represented by several different parts (tooth enamel, dentine, and bone fragments) and/or related sediment matrix elements (coprolites, fish teeth), were involved in the trace element study. Often multiple fragments of the same individual together with dentine-enamel pairs were analyzed and considered separately. The stratigraphic origin of each mammal specimen (i.e., the layer it comes from), therefore is represented by between one and eight sub-samples (see Table 1). Each of these represents the average of 1 to 4 spot analyses (Table 2). Altogether, 67 sub-samples were analyzed, of which 32 are directly from mammal remains, while the rests are from sediment matrix elements related to the mammals. Prior study indicates that samples from the same layers yielded a similar REE distribution (Kocsis et al., 2016), and hence unique mammal fossils (e.g., types specimens) not available for sampling can be represented by geochemical data analyzed from the matrix elements in the sediments attached to these rare fossils.

The trace element concentration data and ratios are listed in Supplementary Material Table-3, and selected ones are plotted in Figures 3-5. A range of elements, such as Sr, Zn, Ba, totREE and U, are compared in the boxplots (Figure 3). Sr is especially enriched in the shark tooth enameloid (average > 2035 ppm), while other types of remains hardly reach 1000 ppm. On average, the zinc concentration is somewhat higher in the enamel and enameloid, while barium is more enriched in the terrestrial remains. Variations of the early diagenetic rare earth elements (REE) and U concentrations within the samples are similar to data already reported from the Ouled Abdoun Basin (Kocsis et al., 2016). For example, the denser enamel/enameloid generally yielded lower concentrations compared to dentine, bones or coprolites. Importantly, all the investigated specimens, the mammals and the marine matrix elements, show very similar REE patterns with a negative Ce-anomaly and heavy REE enrichment. The Ce-anomaly and the Pr-anomaly can be quantified as $Ce/Ce^* = 2Ce_N / (La_N+Pr_N)$ and $Pr/Pr^* = 2 Pr_N/(Ce_N + Nd_N)$, where N denotes the Post-Archean Australian Shale (PAAS) normalized value (McLennan, 1989). These parameters, however reveal subtle variations among the samples, as they link to stratigraphic origin rather than taxon affiliation (Figures 4-6).

4.3. Strontium isotope ratios ($^{87}Sr/^{86}Sr$)

Four mammal specimens from different ages were chosen and altogether nine separated analyses were carried out: four enamel, three dentine and two bones (Table 2, Figure 7).

The $^{87}Sr/^{86}Sr$ ratios vary between 0.707856 and 0.708182, and a clear decreasing trend from enamel through dentine to bones is observed. In addition, twenty-four shark tooth enameloids - 16 from the Ouled Abdoun Basin and 8 from the nearby Ganntour Basin - were measured for $^{87}Sr/^{86}Sr$ ratios, and yielded a range from 0.707714 to 0.707920 (Supplementary Material Table-5). The data are shown in Figure 7, together with a comparison to the global strontium evolution curve for the open ocean (see McArthur et al., 2020).

4.4. Stable isotope analyses ($\delta^{18}O_{PO4}$, $\delta^{13}C$, $\delta^{18}O_{CO3}$)

Ten mammal specimens from five taxa (*D. rebouli,* Hyracoidea indet.*, P. escuilliei, O. grandis*, *E. azzouzorum*; Table 2) were analysed for phosphate oxygen isotopic composition, chiefly in the tooth enamel, but a few dentine and bone samples were analysed as well. No systematic variation was observed among these materials. The $\delta^{18}O_{PO4}$ data vary between 18.0 and 22.6 ‰ and the overall average value is 19.8 ± 1.1 ‰ (n = 19). Individual mean values and taxon averages are shown in Table 2, while the taxon-related variation is plotted in Figure 8. One of the *Daouitherium rebouli* specimens (MNHN.F PM3) yielded the highest $\delta^{18}O_{PO4}$ value (22.3 ± 0.4 ‰, n = 2), while the other specimens (PM65, ML 20269987) of this species vary between 18.6 and 21.2 ‰. Only eight samples were analyzed for isotopic composition in the structural carbonate in the bioapatite ($\delta^{13}C$, $\delta^{18}O_{CO3}$), belonging to four taxa. The $\delta^{13}C$ derived enamel (n = 5) ranged between -7.1 and -8.6 ‰, while a dentine and two bone samples yielded higher values of -6.3, -4.6, and -3.9 ‰, respectively (Table 2, Figure 8). The values of $\delta^{18}O_{CO3}$ ranged between -3.7 and -5.1 ‰ for the enamel, whereas the dentine and the two bones yielded somewhat lower values of -5.6, -5.6, and -5.1 ‰, respectively (Table 2).

5. Discussion

5.1. Terrestrial, marine, and diagenetic signals

Hard tissues (i.e., bones, teeth) of terrestrial and marine animals record the chemical and isotopic signatures of their respective environments, hence when these remains are fossilized the ancient ecological conditions can be traced in the case of no alteration (e.g., Tütken et al., 2006; Kocsis et al., 2007; Domingo et al., 2009; Reynard and Balter, 2014;

317 Akhtar et al., 2020). Generally, freshwater (e.g., terrestrial drinking sources) has a lower F
318 and Sr content than seawater, while Ba is instead expected to be higher in rivers and lakes
319 (White 1998; Bruland and Lohan 2003; Gaillardet et al. 2003). Therefore, these elements can
320 help tracing *in-vivo* preserved environmental signals, and can give information on alteration
321 during fossilization. Moreover, the taphonomic relations of mixed assemblages, such as the
322 one studied here, can be further investigated (e.g., Trueman et al., 2003; Tütken et al.,
323 2008).

324 In this study, the low F and high Ba content, but also the low Ca/P and high $^{87}Sr/^{86}Sr$
325 ratios in the mammal tooth enamel, indicate at least partially preserved *in-vivo* values
326 reflecting a continental source and origin. The higher F and lower Ba concentrations, and Sr-
327 isotope ratios in the mammal dentine and bone that are closer to marine values, are best
328 explained by diagenesis in a seawater-dominated pore fluid (Figures 2-3). The burial
329 condition is also reflected by the chemistry of the marine coprolites (Figure 2), which
330 phosphatized within the sediments (Cosmidis et al., 2013), and yielded similar compositions
331 to those of the mammal bones and dentine. Therefore, the Ca/P ratio and F of these
332 mammal remains were altered in a marine depositional setting. The latter materials have a
333 higher susceptibility to interaction and exchange with the depositional fluid due to their
334 lower crystallinity and density, and originally higher porosity and organic content when
335 compared to the enamel. The higher concentrations of REE and U, and possibly the higher
336 $\delta^{13}C$ and lower $\delta^{18}O_{CO3}$ values, in the dentine and bone are also the result of the postulated
337 structural differences and related diagenesis in a marine pore-fluid (Figure 3 & 8, Table 2).

338 As an *in-vivo* marine environmental end-member, shark tooth enameloid is the best
339 suited material, as it is indicated by the following geochemical data: (1) a high F content, (2)
340 low Ca/P ratios, (3) a high Sr concentration, and (4) very similar $^{87}Sr/^{86}Sr$ ratios to the open
341 seawater of the time (McArthur et al., 2020; see chapter 5.3), and partly also (5) oxic-
342 seawater related REE patterns (Figure 4; Kocsis et al., 2016) (Figure 2).

343 Based on the above observations, enamel/enameloid geochemical values should be used
344 in any ecological and *in-vivo* interpretations. In this sense, the somewhat higher
345 concentrations of Zn in both the mammal enamel and shark tooth enameloid call for further
346 explanation, as these values may link to a common *in-vivo* origin. Zn has been connected to
347 enzymes (e.g., kallikrein - KLK4) that play an important role in mammal tooth enamel
348 formation (amelogenesis). In fact, KLK4 helps in removing organic matter at a later stage, so

as to make the enamel harder (e.g., Simmer et al., 2009; Goetttig et al., 2010). A high Zn concentration has been detected in modern shark enameloid and a similar enzymatic process has been proposed (Kocsis et al., 2015). Therefore, the observed relatively higher Zn concentration in our enamel/enameloid may partly relate to the process of enamel mineralization during amelogenesis. For other *in-vivo* interpretations based on the stable isotope and strontium isotope ratios, see Sections 5.3 and 5.4.

5.2. REE element taphonomy and stratigraphy

The rare earth element content of fossil bioapatite is predominantly of early diagenetic origin and can reflect the burial fluid's REE composition (e.g., Elderfield and Pagett, 1986; Trueman and Tuross, 2002). This signature of fluid composition is frequently used to address taphonomic questions related to fossil vertebrates (e.g., Staron et al., 2001; Trueman et al., 2003; MacFadden et al., 2007; Tütken et al., 2008; Botfalvai et al., 2021) or to assess palaeoenvironmental conditions (e.g., Picard et al., 2002; Shield and Webb, 2004; Kocsis et al., 2007, 2009; Žigaitė et al., 2016, 2020). From the Ouled Abdoun and Ganntour basins in Morocco, Kocsis et al. (2016) tested over 200 bioapatite specimens, and this database has been extended here (Supplementary Material Table-1). Based on the REE concentrations, their variations along the phosphate series, and their variations within the specimens, any late diagenetic overprint or fractionation along the REE series is ruled out (e.g., Kocsis et al., 2016). Therefore, the REE patterns we have obtained, and the related elemental ratios, can confidently be linked to the depositional environment.

As was the case in the prior study, the REE content of the fossils analyzed here increases from enamel/enameloid to coprolite, dentine, and bone, which, as mentioned earlier, reflects original structural and compositional (i.e., organic content) differences among these materials. However, a very important fact is that all the samples (in this study and in Kocsis et al. 2016), yielded similar REE distributions, which mimic oxic seawater patterns (i.e., a negative Ce-anomaly and HREE enrichment) regardless of the material and taxa involved (Figure 4). This further supports the conjecture that the terrestrial mammal remains were fossilized within a marine depositional setting together with the marine fossils, and that they gained their REE content from seawater dominated pore fluids. An additional implication is that the mammal carcasses were most likely directly transported into the marine realm, without any previous terrestrial depositional site in the hinterland. This is

compatible with the hypothesis that the terrestrial mammals were drained as floated bodies from the nearby hinterland by local rivers in the Ouled Abdoun phosphate basin, shortly after their deaths (Gheerbrant et al., 2003).

Despite the very similar REE patterns, the samples do vary in their Ce/Ce* and Pr/Pr* ratios, which together express the degree of Ce-anomaly (Figure 4) (Bau and Dulski, 1996). The variations in the ratios are time related, meaning that samples from the same bed cluster around similar values. Therefore the REE distribution of any remains from the sediment matrix, such as coprolites, pellets or small teeth, attached or embedded with the mammal fossils, represents these rare fossils with no bias (see Table 1).

The few mammal samples and/or their sediment matrix whose stratigraphic origins were previously known perfectly match the reference Ce/Ce* curve established by Kocsis et al. (2016) (Figure 5). Moreover, taxa with presumably Paleocene (e.g., Ocepeiidae spp., *Abdounodus*, *Eritherium*) or Eocene (e.g., *Phosphatherium*, *Daouitherium*, *Stylolophus* spp.) ages fit in the corresponding data cluster (Figure 4).

The background Ce/Ce* dataset for the Ouled Abdoun Basin allows for comparison of the mammal-derived data with their possible stratigraphic positions (Figures 4-6). The sedimentary section was divided into ten chemostratigraphic horizons based on the Ce/Ce* variation and major sedimentological units including the three bone-beds (Horizons 3, 5, and 7), where mammal remains presumably were found. The variance and mean of the Ce/Ce* values for the consecutive layers were compared using the F and Student's-t tests respectively (Supplementary Material Table-6), and these yielded significant differences (Student's t-test $p < 0.05$) with the exceptions of the top of Bed-IIb (Horizon 8) and the *Eritherium* bone bed (Horizon 7) ($p = 0.604$). Then, in order to trace the possible stratigraphic origin of the mammals, each mammal data-group ($n > 2$) was compared to the respective horizons using one-way ANOVA (i.e., Eocene mammals to Horizons 1 - 5; Paleocene mammals to Horizons 5 - 10), and the underlying differences in the mean Ce/Ce* values were checked using Tukey's pairwise tests (Table 3).

5.2.1 Paleocene taxa

The three specimens of *Eritherium azzouzorum* (PM40; MNHN.F.PM42; PM100a see Table 1) found in the *Eritherium* bone bed fit the background Ce/Ce* data from this horizon (Horizon 7). However, they are also statistically similar to the horizons below and above. The

Ce/Ce* data of the taxa with unknown provenance revealed that their origin is restricted to the interval between the very top of Bed IIb and the base of Bed IIa, including the *Eritherium* bone bed (chemostratigraphic Horizons 6-8 i.e., early Thanetian–Selandian-?latest Danian age)(Figure 6, Table 3). This suggests that these mammal specimens do not come from younger Paleocene bone beds such as the big coprolite bone bed (base of Horizon 5), which was the suspected provenance of one of the *O. grandis* specimens (PM66) based on information from local collectors. Fossil collectors usually target higher accumulations of bones (i.e., the bone beds) to find unique specimens, hence the *Eritherium* bone bed (Horizon 7) could be the most important source of these fossils. However, our results support the hypothesis that some mammal specimens such as MNHN.F PM39 of *O. grandis*, – and solely based on its Ce/Ce* ratio – maybe even the MNHN.F PM42 of *E. azzouzorum*, might be derived from layers overlying the base of Bed IIa (Horizon 6) (Figure 6). Among the Ocepeiidae, the overlapping probabilities of their stratigraphic provenance indicate that the smaller *O. daouiensis* and the larger *O. grandis* were co-existing, therefore refuting the possibility that they were successive chronospecies (Table 3-4, Figure 5). For the specimens where only one Ce/Ce* data point is available (Ocepeiidae? – MHNM.KHG.224 and *Abdounodus hamdii* - PM67), the result agree with the suggested origin in Horizons 6-8.

5.2.2 Eocene taxa

The Eocene taxa reveal a wider range of possible provenance beds, based on the statistical analysis (Table 3). This relates partly to the fact that the Ce/Ce* values are increasing in the youngest beds, and so they overlap with some of the older levels, while the latest Paleocene beds (top Bed IIa – Horizon 5) show very similar values to those of the early Ypresian beds (Figure 5). An exception is Horizon 4, with few specimens (the very base of intercalary II/I), which clearly does not match any of the taxa due to its high Ce/Ce* values, and which are similar to the older Paleocene data series. This small spike in the Ce/Ce* values may reflect reworked older specimens from Bed IIa, as has been recognized also by Gheerbrant et al. (2003), and/or a very brief episode of less oxic, somewhat confined conditions (probably after the PETM event) (Kocsis et al., 2016).

On the other hand, most of the taxa show significant undifferentiated similarities to the whole range of chemostratigraphic Horizons 1, 3, and 5, i.e. upper Thanetian-Ypresian (Figure 6). Unfortunately, the Ce/Ce* chemostratigraphic approach alone could not help to

445 define the exact provenance of the mammal taxa in these three horizons, so additional
446 information from the sediment matrix and related selachian fauna (i.e., shark and ray) are
447 needed for further stratigraphic assignment.
448 The origin of the few *Phosphatherium escuilliei* specimens (MNHN.F PM14 and MNHN.F
449 PM17) is known for certain to be the *Otodus obliquus* bone bed in the intercalary phosphate
450 Beds II/I (i.e., base Horizon 3) (Table-1, Gheerbrant et al., 2005), but no trace element
451 analyses were carried out on these specimens. However, the specimens of this species with
452 unknown provenance (MNHN.F PM25, OCP DEK/GE336) yielded Ce/Ce* data fitting an
453 origin in Horizon 3, which includes the *Otodus obliquus* bone bed (Figure 6).
454 The sediment matrix and the related selachian remains assigned the *Stylolophus minor*
455 (OCP DEK/GE 668) specimen to the *Otodus obliquus* bone bed, a conclusion which is further
456 confirmed by its Ce/Ce* values (Figure 5). Selachian taxa found in the matrix of the other
457 specimen of *S. minor* (MNHN.F PM30) are also compatible with Horizon 3 (see
458 Supplementary Material Table-7). The Ce/Ce* data for the other specimens analyzed
459 (MNHN.F PM30 & OCP DEK/GE 667) would also match an origin in Horizon 3 (early Ypresian)
460 (Figure 6).
461 For these two species (*P. escuilliei* and *S. minor*), however, the general similarity in the
462 Ce/Ce* values to the latest Paleocene beds (Horizon 5: top Bed IIa including the big
463 coprolite bone bed) raise the possibility that some of these specimens may have belonged
464 to the older Horizon 5. Thus, we cannot exclude that these species have crossed the PETM
465 boundary. It must be mentioned that the provenance of *P. escuilliei* and *S. minor* from
466 Horizon 1 (Table 3) is completely rejected here, due to the lack of strong similarities with the
467 thick succession of Horizon 2, which stratigraphically follows Horizon 3 (Figure 5).
468 *Stylolophus major* (MNHN.F PM53) has the highest probability of occurrence in the
469 youngest Horizon 1 (the sillons beds – Table 3, Figure 6). If it is correct, it would be the
470 stratigraphically youngest mammal recovered in the Ouled Abdoun phosphate series. A
471 stratigraphic origin of *S. major* from the sillons beds is further supported by its larger size
472 and its more derived morphology with respect to *S. minor*, and also by the chert content
473 and the selachian assemblage found in its matrix (Gheerbrant et al., 2018, 2020). In fact, this
474 species yielded very different Ce/Ce* and Pr/Pr* ratios from the rest of the mammals (see
475 Figure 4d), and when Tukey's pairwise comparison is applied to all these younger taxa it
476 reveals that *S. major* is significantly different from the rest of the remains ($p < 0.05$, Table 4),

which further supports its younger origin in the phosphate series (i.e., Horizon 1 – late Middle Ypresian).

For *Daouitherium rebouli*, the matrix data and related fauna suggest an origin in Bed 0 or Bed 0' (Horizon 2) (see Supplementary Material Table-7). Generally, our Ce/Ce* data support this scenario, although Horizons 1 and 3 yielded a higher probability match. Moreover, these specimens do not differ in their Ce/Ce* values from those of *P. escuilliei* and *S. minor* (Table 4). The Ce/Ce* data match Horizon 5 (Paleocene), but the attached matrix-type and related selachian fauna preclude this scenario (see Table 3). *Daouitherium* is the largest proboscidean from the Ouled Abdoun Basin and most probably evolved somewhat later than *Phosphatherium*, so the younger age might be possible too (Gheerbrant et al., 2002). Here we propose an origin in the interval from the top Horizon 3 to Horizon 2 (middle Ypresian) (see the grey shaded area in Figure 5).

The difficulties in pinpointing more precise stratigraphic provenances based on only the Ce/Ce* data is clear from the above example, and the limitations of the method are further highlighted by the Hyracoidea specimen (MNHN.F PM52), for which no additional matrix related information is available. The similar probability pattern to the *D. rebouli* specimens (Table 3) may suggest a similar origin; while significant differences from the holotype of *S. major* (Table 4) would argue against a provenance in Horizon 1. Therefore, we propose here a possible origin for the Hyracoidea from the top of Horizon 3 to Horizon 2 (middle Ypresian).

To sum up, in general the chemostratigraphic approach supports the previous assumptions made about the provenances of the mammal taxa investigated here, but it has also shed light on certain peculiarities such as (1) the Ocepeiidae species, in particular *O. daouiensis* and *O. grandis*, coexisted in the Ouled Abdoun phosphate series for an undetermined period from the latest Danian to the early Thanetian; (2) the Ypresian species *P. escuilliei* and *S. minor* might have already evolved in the latest Paleocene; (3) *Stylolophus major* is the youngest and only known mammal taxon derived from the highest phosphorite sillons beds (late Middle Ypresian). Based on the Ce/Ce* data and additional matrix and biostratigraphic (i.e., selachian fauna) information, the most probable stratigraphic origin of the mammal specimens are marked by the grey areas in Figure 6.

5.3. Strontium isotope ratios in terrestrial and marine fossils

The Sr that is biologically available in a terrestrial environment is affected by the local geology, and it is incorporated into the skeletal tissues via ingestion without fractionation along the food chain (e.g., Blum et al., 2000). Therefore, the strontium isotope ratios ($^{87}Sr/^{86}Sr$) of fossil terrestrial mammals are often used to trace migration patterns (e.g., Hoppe et al., 1999; Tütken et al., 2006; Arppe et al., 2009). On the other hand, in the open marine realm the seawater has a constant $^{87}Sr/^{86}Sr$ ratio due to the long residence time of Sr. However, on longer timescale the ratio does vary, and this variation is the basis of strontium isotope stratigraphy (e.g., McArthur et al. 2020). Dating marine rocks with well-preserved fish remains is one widely used approach (e.g., Ingram 1995; Kocsis et al., 2013; Harrell et al., 2016), while in the case of mixed terrestrial and marine assemblages, taphonomy of the remains can give further information.

Our $^{87}Sr/^{86}Sr$ analyses from the Ouled Abdoun basin yielded differences between the continental and marine taxa, with the mammal fossils in general having higher ratios (Figure 7a). The highest ratios come from mammal enamel that represents possibly unaltered terrestrially-derived and ingested Sr (i.e., *in-vivo*), which reflects the hinterland geology of the time. The $^{87}Sr/^{86}Sr$ ratios decrease through dentine to the bone samples, which approaches the values of the open ocean (Figure 7a). This decreasing trend within the different types of mammal remains clearly indicates diagenesis in a marine depositional environment, and as mentioned earlier this has an important taphonomic message. The remains were originally deposited in a marine setting and they are not reworked from previous deposits.

On the other hand, the data derived from the shark tooth enameloid more or less follow the global open ocean Sr-evolution curve. This is most noticeable for the latest Paleocene and Eocene where the Sr-isotope ages agree with other chemostratigraphic data (Yans et al., 2014; Kocsis et al., 2014a). However, the rest of the Paleocene and part of the Cretaceous samples yielded $^{87}Sr/^{86}Sr$ ratios that cannot fit the global Sr-isotope curve because their values are too high (Figure 7). The most plausible interpretation is that these samples were altered during early diagenesis. A high $^{87}Sr/^{86}Sr$ ratio could have derived from a terrestrial source, as attested by the mammal enamel's high $^{87}Sr/^{86}Sr$ values. However, there is no evidence of strong continental input in the sedimentary record of the phosphates series, which corresponds mostly to non-clastic deposits of biogenic origin (i.e.,

541 marine bioproductite see Lucas and Prevôt-Lucas, 1995). The continental influence is
542 marked there only by occasional rare terrestrial fossils in the phosphate levels. The
543 terrestrial sediment input in the Moroccan phosphate basins was low, due maybe to the flat
544 topography in the hinterland (low hydrodynamism and erosion) and perhaps also to the
545 filtering role of coastal mangroves (e.g., Fechner, 1988). However, the river water and/or
546 sub-terrain water draining from the hinterland towards the basin may have had some
547 effects, at least in the transportation of the floating bodies/carcasses of the Ouled Abdoun
548 mammals (Gheerbrant et al., 2003).
549 The REE element patterns, however, were still compatible with oxic seawater (Figure 4).
550 Though the Ce/Ce* ratios are somewhat higher here than in the younger samples (Figure 5),
551 the stratigraphic changes in these values were interpreted as a reflection of the enhanced
552 opening of the Atlantic Ocean and hence a better connection with the global oceanic
553 circulation (Kocsis et al., 2016). In this sense the $^{87}Sr/^{86}Sr$ data of the Cretaceous and older
554 Paleocene samples could indicate somewhat more restricted conditions in which seawater
555 was slightly locally controlled. First-order sea-level changes during the late Cretaceous and
556 early Paleogene indicate global regression (e.g., Hardenbol et al., 1998; Snedden and Liu,
557 2010; van der Meer et al., 2017), which could support the semi-confined situation in the
558 Moroccan phosphate basins. Interestingly, the $^{87}Sr/^{86}Sr$ data reported from foraminifera
559 from the South Atlantic (Walvis Ridge) also yielded rather higher ratios than the global
560 ocean Sr-isotope curve during this part of the Paleocene (Hodell et al., 2007). Even if some
561 samples were clearly affected by diagenesis the lowest Sr-isotopic ratios have a perfect fit
562 with McArthur's curve between 52 and 58 Ma (Figure 7b), but the older samples are above
563 the curve at the Walvis Ridge as well. This might hint at a common cause altering the Sr-
564 budget and its mixing in the Central and South Atlantic, which may have been related to the
565 formation of wider scales of global oceanic circulation. Nevertheless, better suited samples
566 covering larger regions are needed to seriously assess this scenario.
567
568 *5.4. Mammal ecology based on stable isotope chemistry*
569 The oxygen and carbon isotopic compositions of fossil mammal teeth are often used for
570 palaeoecological and palaeoenvironmental reconstructions (e.g., Ayliffe et al., 1994; Kohn
571 and Cerling, 2002; Amiot et al., 2004), even for extinct taxa of the Paleocene and Eocene for
572 which the physiology of the animals is more difficult to assess (e.g., Liu et al., 2008; Secord

et al., 2008; Kocsis et al., 2014b; Mahboubi et al., 2014; Tütken, 2014). Nevertheless, based on the tooth morphology the mammals from the Ouled Abdoun Basin investigated here were all herbivores (Ypresian proboscideans are especially folivorous specialists). Their body fluid $\delta^{18}O$ depends on the ingested water, which mainly came from drinking sources and/or dietary plant water, while their $\delta^{13}C$ was entirely driven by their diet and can be related to the palaeoflora (e.g., Kohn and Cerling, 2002). The growth of teeth and bones record these ecological parameters, and can be used to gain information about the past environment. The teeth and bones are composed of bioapatite with a simplified formula of $Ca_5(PO_4, CO_3)_3(OH, CO_3)$. From the oxygen bearing ions, the phosphate ion dominates the apatite structure and is considered to be the most resistant to diagenesis due to the strong P-O bond. Therefore, the phosphate oxygen isotopic composition ($\delta^{18}O_{PO4}$) can provide the most reliable ecological information. To further evaluate possible alterations, enamel, dentin and bone can be analyzed separately and compared, with the enamel considered to be less prone to diagenetic alteration (e.g., Zazzo et al., 2004). The $\delta^{18}O_{PO4}$ data from the Moroccan mammals do not show consistent variations across these materials, but the $\delta^{13}C$ of *O. grandis* and *P. escuilliei* clearly point towards higher values in the less dense material of bone and dentine (Figure 8). This can be interpreted as meaning that the $\delta^{18}O_{PO4}$ data are more robust across the various materials; however the isotope values from the structural carbonate underwent partial interaction and exchange with the marine pore fluid in the depositional environment. For this reason, only the enamel data are taken into account when the ecology of these ancient mammals is discussed, even for the $\delta^{18}O_{PO4}$ results.

The overall average $\delta^{18}O_{PO4}$ value for the enamel is 20.0 ± 1.3 ‰ (n = 12), and no obvious species-specific variations occur. The largest variation is between two specimens of *Daouitherium rebouli* (MNHN.F PM3 and PM65), with a nearly 3 ‰ difference in their enamel values (Figure 8). The relationship between mammal $\delta^{18}O_{PO4}$ and the local meteoric water (i.e., consumed water) can be taxon specific and dependent also on the relative humidity (e.g., Kohn, 1996; Ayliffe et al., 1994; Kohn and Cerling, 2002). This can be complicated further by the migration of animals, seasonal variations, and/or locally available water sources that are different from the local meteoric water. Moreover, the physiology of the investigated taxa is hard to assess, and for these reasons Amiot et al. (2004)'s globally compiled mammal database and latitude adjusted $\delta^{18}O_{PO4}$ versus meteoric water correlation

604 is used here, with the assumption that the ancient mammals' body fluids were affected by
605 the local meteoric fluid (i.e., drinking water or plant water). This would yield an average of -
606 4.2 ± 1.3 ‰ (n = 12) local meteoric water isotopic composition, which in turn can be linked
607 to a mean annual temperature of 20.4 ± 3.0 °C (n = 12) (see Amiot et al., 2004) for the late
608 Paleocene and early Eocene (Figure 8). This is about 2-3 °C degrees higher than today's MAT
609 for the coastal area of Morocco (e.g., Agadir-Casablanca, see climate-data.org). Considering
610 the palaeolatitudinal temperature gradient for a greenhouse climate regime (Amiot et al.,
611 2004) and the fact that the studied sites were not much further south (~22°-24°N, see van
612 Hinsbergen et al., 2015) than today, the absolute MAT result we obtained seems
613 reasonable. Nevertheless, the higher isotopic composition in the bioapatite indicates a
614 higher isotopic composition in the ingested water, which in turn reflects a higher MAT
615 (Figure 8). The high $\delta^{18}O_{PO4}$ values for one of the *D. rebouli* (MNHN.F PM3) and Hyracoidea
616 (MNHN.F PM52) teeth may reflect the effects of the Early Eocene Climatic Optimum (EECO),
617 with arelated global temperature rise and/or enhanced dryer periods (i.e., more
618 evaporation of the drinking sources). However, only a few samples were analyzed and the
619 high $\delta^{18}O_{PO4}$ values and related temperature calculations might be biased by the migration
620 of the animals or strong evaporation of the local drinking source. Geochemical analysis of
621 the sediments and the marine fossils had also detected the EECO event in the phosphorite
622 series (Yans et al., 2014; Kocsis et al., 2014). Moreover, the stratigraphic average MATs
623 reveals a rise of about 5 °C degree from the early Ypresian to mid-Ypresian (Figure 8), which
624 agrees well with the peak of the EECO and related ΔMAT estimates (e.g., Hyland et al.
625 2016). If these analyses indeed reflect the EECO, then the proposed stratigraphic origin of
626 these taxa (*D. rebouli* & Hyracoidea) in Horizons 3 (upper part) and 2 is further confirmed
627 (see section 4.2 and Figure 6).
628 The average enamel $\delta^{13}C$ value is -7.9 ± 0.8 ‰ (n = 5), which can be translated to a
629 consumed plant isotopic composition of -22 ± 0.8 ‰ (e.g., Kohn and Cerling, 2002; Figure 8).
630 This mean value is at the very high end of a C3 palaeoflora, and because the C4
631 photosynthetic pathway was not yet widespread (i.e., high $\delta^{13}C_{plant}$), this suggests a very dry
632 Thanetian-middle Ypresian local continental palaeoecosystem with mean annual
633 precipitation well below 500 mm (Kohn, 2010). A dry arid early Eocene climate was also
634 suggested by palynology and palaeobotanic finds in the Moroccan south Atlas, which

indicated mangrove and marsh vegetation along the palaeo-coast, together with a fairly dry and scarcely vegetated hinterland (Mohr, 1986; Mohr and Fechner, 1986; Fechner, 1988). Mangrove vegetation along the coast line is also predicted by models (Descombes et al., 2018; Couvreur et al., 2021). The presence of early diagenetic dolomite and gypsum in some of these deposits were also interpreted as a consequence of an arid climate during the Ypresian, and only a low amount of seasonal precipitation was proposed (e.g., Mohr, 1986; Fechner, 1988). In addition, the rarity of detritic (clastic) material in the phosphate basins (Lucas and Prevôt-Lucas, 1995), and the high quantity of palygorskite clay mineral in the Paleogene deposits in the Atlas (Daoudi, 2004; Knidiri et al., 2014) and offshore Morocco (e.g., Chamley et al., 1980), would further suggest a dry semi-arid late Paleocene - Ypresian climate in the region. By contrast, Herbig and Gregor (1990) have advocated a tropical humid climate based on the discovery of mangrove macro-plant remains of *Nypa* palms from Thanetian-Ypresian levels in the Ouarzazate Basin, based on a re-evaluation of early available data.

In the view of the mammal enamel $\delta^{13}C$ values from the Ouled Abdoun Basin, the ingested plants must have lived in water-stressed, and maybe also salinity-stressed (i.e., mangrove vegetation, e.g., Wei et al., 2008) environment, supporting the hypothesis of arid late Paleocene - Ypresian climatic conditions in the region. The minimal variation in the $\delta^{13}C$ values through time could reflect a steady dry ecosystem along the Moroccan coastline during the Paleocene-Eocene. Still, the EECO warm period may have stressed the palaeoflora further, and even somewhat higher values of $\delta^{13}C$ may be expected (e.g., even more water stress, Farquhar et al., 1989). However, this may have been compensated by a higher relative humidity and / or higher atmospheric pCO_2 during the EECO (Pearson and Palmer, 2000; Schubert and Jahren, 2002). The EECO warming is likely also to have driven an evolution to increased size the Ouled Abdoun mammals (e.g., Yans et al., 2014). The embrithopods lineage *S. minor- S. major* (Gheerbrant et al., 2020) records a significant increase in size during the early-middle Ypresian. Similar size changes are observed between *Phosphatherium* and *Daouitherium*, however with much less stratigraphic difference between these taxa as inferred here (Figure 6).

6. Conclusions

The rare but diverse terrestrial mammal fossils from the Ouled Abdoun phosphorite are proven to have a similar diagenetic history to that of the marine fossils. This is reflected by a similar REE distribution and stratigraphy matched Ce/Ce* and Pr/Pr* ratios. The Ce/Ce* variation along the phosphate series either confirmed previous known origins or helped to estimate the stratigraphic provenance of the Ouled Abdoun mammal specimens whose origin was unknown. Exchanges with marine pore fluid affected the enamel, dentine, and bone differently, with the enamel being the most robust to alteration, and hence the best to use for investigation of the palaeoenvironment of the African Paleogene mammals from the Ouled Abdoun sites.

This study has identified ten chemostratigraphic horizons in the Maastrichtian-Ypresian phosphates series of the Ouled Abdoun Basin. It confirms most of the previously proposed age determinations for the mammals found in the Ouled Abdoun Basin, but with some corrections and additions. One new conclusion is that all the Paleocene mammal material studied here ranges from the Selandian to the lower Thanetian (uppermost Bed IIb to the base of Bed IIa). In particular, *O. grandis* does not come from the upper part of Bed IIa (late Thanetian) but is actually a coexisting lineage with *O. daouiensis*, which highlights the little-known radiation of the stem paenungulates. The study suggests that some mammal species might have a wider stratigraphical extension than previously known, including across the PETM. However, as the Ouled Abdoun mammal material remains scarce, it is unknown if this relates to the presence of undetermined chronospecies or to the succession of intraspecific diachronic populations. Chemostratigraphic results indicate that the embrithopod *S. major* likely comes from the uppermost phosphates levels (late Middle Ypresian) of the Ouled Abdoun series, and is the youngest Paleogene mammal known in the Ouled Abdoun Basin.

While the mammal enamel yielded the highest $^{87}Sr/^{86}Sr$ ratios, indicating the composition of the hinterland rocks (a terrestrial Sr-source), the ratios for the shark tooth enameloid from the latest Paleocene to early Eocene are compatible with the open ocean Sr isotope ratios of the time. Older marine fossils deviate from the global Sr-isotope curve, which most probably reflects alteration or may link to somewhat restricted conditions and a variable Sr-budget in the African coastal basins of the Atlantic Ocean. The enamel derived oxygen and carbon isotopic compositions of the Ouled Abdoun mammal teeth point to warm and arid climatic conditions along the Atlantic palaeocoast of North Western Africa. In addition, an

increase about 5 °C degrees in MAT was recorded by the mid-Ypresian, which is linked to the EECO. Our geochemical study of the Ouled Abdoun fossils provides support for the evolution of endemic African lineages of placental mammals, such as the early embrithopod *Stylolophus*, during the EECO event.

Acknowledgements

The research was conducted under L.K.'s Ambizione research grants (Nr. PZ00P2_126407 & PZ00P2_145115/1 – Switzerland), but in the later phase of the project LK also received support from his URC Grant from Universiti Brunei Darussalam (UBD/PNC2/2/RG/1(325)). The help from both funding agencies is much appreciated. This study benefited from the paleontological "Phosphapal" collaborative Agreement with the Ministère de l'Energie, des Mines, de l'Eau et de l'Environnement (MEMEE), the Office Chérifien des Phosphates (OCP SA) of Morocco, the Muséum National d'Histoire Naturelle (MNHN, Paris), and the Universities Cadi Ayyad (Marrakech, Morocco) and Chouaıb Doukkali (El Jadida, Morocco). We are most grateful to the Geological Survey of the OCP mining centre of Khouribga for help with the field work. Identification of the matrix related selachian fauna by Prof. Henri Cappetta (CNRS, Université de Montpellier II, France) is much appreciated. Constructive comments on a previous version of the manuscript by the editor Thomas Algeo, and three reviewers, Živilė Žigaitė and 2 anonymous ones, are much appreciated. We thank Malcolm R. Anderson for proofreading the updated manuscript.

References

Akhtar, A.A., Santi, M.L., Griffiths, L.M., Becker, M., Eagle, A.R., Kim, S., Kocsis, L., Rosenthal, Y., Higgins, J.A., 2020. A record of the $\delta^{44}/^{40}$Ca and [Sr] of seawater over the last 100 million years from fossil elasmobranch tooth enamel. Earth and Planetary Science Letters 543, doi.org/10.1016/j.epsl.2020.116354.

Amiot, R., Lecuyer, C., Buffetaut, E., Fluteau, F., Legendre, S., Martineau, F., 2004. Latitudinal temperature gradient during the Cretaceous Upper Campanian Middle Maastrichtian: δ^{18}O record of continental vertebrates. Earth Planet. Sci. Lett. 226, 255–272. http://dx.doi.org/10.1016/j.epsl.2004.07.015.

Arambourg, C., 1952. Les vertébrés fossiles des gisements de phosphates (Maroc-Algérie-Tunisie). Notes Mémoires du Service géologique du Maroc 92, pp. 1–372.

Arppe L., Karhu J.A., Vartanyan S.L., 2009. Bioapatite ^{87}Sr/^{86}Sr of the last woolly mammoths – implications for the isolation of Wrangel Island. Geology 37, 347–350.

Ayliffe, L.K., Chivas, A.R., Leakey, M.G., 1994. The retention of primary oxygen isotope compositions of fossil elephant skeletal phosphate. Geochim. Cosmochim. Acta 58, 5291–5298. http://dx.doi.org/10.1016/0016-7037(94)90312-3.

Bardet, N., Gheerbrant, E., Noubhani, A., Cappetta, H., Jouve, S., Bourdon, E., Pereda Suberbiola, X., Jalil, N.-E., Vincent, P., Houssaye, A., Solé, F., El Houssaini, Kh., Adnet, S., Rage, J.-C., Lapparent de Broin, F., Sudre, J., Bouya, B., Amaghzaz, M., Meslouh, S., 2017. Les vertébrés fossiles des phosphates crétacés-

737 paléogènes (72,1-47,8 Ma) du Maroc, in Zouhri, S. ed., Paléontologie des Vertébrés du Maroc: état des
738 connaissances. Mémoire de la Société Géologique de France, v. 180, p. 351–452.
739 Bau, M., Dulski, P., 1996. Distribution of yttrium and rare-earth elements in the Penge and Kuruman iron-
740 formations, Transvaal Supergroup, South Africa. Precambrian Res. 79, 37–55.
741 Blum, J.D., Taliaferro, E.H., Weisse, M.T., Holmes, R.T., 2000. Changes in Sr/Ca, Ba/Ca and 87Sr/86Sr ratios
742 between two forest ecosystems in the northeastern USA. Biogeochemistry 49, 87–101.
743 Botfalvai, G., Csiki-Sava, Z., Kocsis, L., Gáspár, A., Magyar, J., Bodor, R.E., Țabără, D., Ulyanov, A., Makádi, L.,
744 2021. X' marks the spot! Sedimentological, geochemical and palaeontological investigations of Late
745 Cretaceous (Maastrichtian) vertebrate fossil localities from Vălioara Valley (Densus-Ciula Formation,
746 Hateg Basin, Romania). Cretaceous Research, 123.
747 Bourdon, E., Bouya, B., Iarochene, M. 2005. Earliest African neornithine bird: A new species of
748 Prophaethontidae (Aves) from the Paleocene of Morocco. Journal of Vertebrate Paleontology, 25 (1),
749 157–170.
750 Bruland, K.W., Lohan, M.C., 2003. Controls of Trace Metals in Seawater. In: Holland, H.D., Turekian, K.K. (eds)
751 Treatise on Geochemistry, vol. 6. pp 23–47.
752 Cappetta, H., Bardet, N., Pereda-Suberbiola, X., Adnet, S., Akkrim, D., Amalik, M., Benabdallah, A., 2014.
753 Marine vertebrate faunas from the Maastrichtian phosphate deposits of the Benguérir area (Ganntour
754 Basin, Morocco): biostratigraphy, palaeobiogeography and palaeoecology. Palaeogeogr. Palaeoclimatol.
755 Palaeoecol. 409, 217–238.
756 climate-data.org
757 Chamley H., Giroud d'Argoud G., Robert C., 1980. Clay mineralogy of Cretaceous and Cenozoic sediments off
758 the Moroccan margin, Deep Sea Drilling Project sites 415, 416. Initial Rep. Deep Sea Drilling Proj., 50,
759 715–721.
760 Cosmidis, J., Benzerara, K., Menguy, N., Arning, E., 2013. Microscopy evidence of bacterial microfossils in
761 phosphorite crusts of the Peruvian shelf: Implications for phosphogenesis mechanisms. Chemical
762 Geology, 359, 10–22.
763 Couvreur, T.L.P., Dauby, G., Blach-Overgaard, A., Deblauwe, V., Dessein, S., Droissart,V., Hardy, O.J., Harris,
764 D.J., Janssens, S.B., Ley, A.C., Mackinder, B.A., Sonké, B., Sosef, M.S.M., Stévart, T., Svenning, J.-C.,
765 Wieringa, J.J., Faye, A., Missoup, A.D., Tolley, K.A., Nicolas, V., Ntie, S., Fluteau, F., Robin, C.,
766 Guillocheau, F., Barboni, D., Sepulchre, P., 2021. Tectonics, climate and the diversification of the
767 tropical African terrestrial flora and fauna. Biol. Rev. 96, 16–51.
768 Daoudi L., 2004. Palygorskite in the uppermost Cretaceous-Eocene Rocks from Marrakech High Atlas, Morocco.
769 Journal of African Earth Sciences, 39, 353–358.
770 Descombes, P., Gaboriau, T., Albouy, C., Heine, C., Leprieur, F., Pellissier, L., 2018. Linking species
771 diversification to palaeo-environmental changes: a processbased modelling approach. Global Ecology
772 and Biogeography 27, 233–244.
773 Domingo, L., Cuevas-González, J., Grimes, S.T., Hernández Fernández, M., López-Martínez, N., 2009. Multiproxy
774 reconstruction of the paleoclimate and paleoenvironment of the Middle Miocene Somosaguas site
775 (Madrid, Spain) using herbivore tooth enamel. Palaeogeogr. Palaeoclimatol. Palaeoecol., 272, 53–68.
776 El Assel, N., Kchikach, A., Durlet, C., AlFedy, N., El Hariri, K., Charroud, M., Jaffal, M., Jourani, E., Amaghzaz, M.,
777 2013. Mise en évidence d'un Sénonien gypseux sous la série phosphatée du bassin des Ouled Abdoun:
778 Un nouveau point de départ pour l'origine des zones dérangées dans les mines à ciel ouvert de
779 Khouribga, Maroc. Estudios Geológicos, 69(1), 47–70. https://doi.org/10.3989/egeol.40781.168
780 Elderfield, H., Pagett, R., 1986. Rare earth elements in ichthyoliths: variations with redox conditions and
781 depositional environment. Sci. Total Environ. 49, 175–197.
782 El Haddi, H., 2014. Les silicifications de la série phosphatée des Ouled Abdoun (Maastrichtien-Lutétien Maroc):
783 Sédimentologie, Minéralogie, Géochimie et Contexte Génétique, [PhD Thesis]: Université Hassan II de
784 Casablanca, Faculté des Sciences Ben M'Sik, 135 p.
785 Farquhar G.D., Ehleringer J.R., Hubick, K.T., 1989. Carbon isotope discrimination and photosynthesis. Ann. Rev.
786 Plant Physiol. Plant Mol. Biol. 40, 503–537.
787 Fechner, G.G., 1988. Selected palynomorphs from the Lower to Middle Eocene of the south Atlas Border Zone
788 (Morocco) and their environmental significance. Palaeogeogr. Palaeoclimatol. Palaeoecol. 65, 73–79.
789 Gaillardet, J., Viers, J., Dupré, B., 2003. Trace Elements in River Waters. In: Holland, H.D., Turekian, K.K. (eds)
790 Treatise on Geochemistry, vol. 5. Pp. 225–272.
791 Gheerbrant, E., 2009. Paleocene emergence of elephant relatives and the rapid radiation of African ungulates.
792 Proceedings of the National Academy of Sciences 106, 10717–10721.

Gheerbrant, E., Sudre, J., Cappetta, H., Bignot, G., 1998. *Phosphatherium escuilliei* du Thanétien du bassin des Ouled Abdoun (Maroc), plus ancien proboscidien (Mammalia) d'Afrique. Geobios 30, 247–269.
Gheerbrant, E., Sudre, J., Iarochene, M., Moumni, A., 2001. First ascertained African "condylarth" mammals (primitive ungulates : cf. Bulbulodentata & cf. Phenacodonta) from the Earliest Ypresian of the Ouled Abdoun Basin, Morocco. Journal of Vertebrate Paleontology 21, 107–118.
Gheerbrant, E., Sudre, J., Cappetta, H., Iarochène, M., Amaghzaz, M., Bouya, B., 2002. A new large mammal from the Ypresian of Morocco: Evidence of surprising diversity of early proboscideans. Acta Palaeontologica Polonica. 47 (3), 493–506.
Gheerbrant, E., Sudre, J., Cappetta, H., Mourer-Chauvire, C., Bourdon, E., Iarochene, M., Amaghzaz, M., Bouya, B., 2003. Les localités à mammifères des carrières de Grand Daoui, Bassin des Ouled Abdoun, Maroc, Yprésien : premier état des lieux. Bulletin de la Société Géologique de France 174, 279–293.
Gheerbrant, E., Sudre, J., Tassy, P., Amaghzaz, M., Bouya, B., Iarochène, M., 2005. "Nouvelles données sur *Phosphatherium escuilliei* (Mammalia, Proboscidea) de l'Eocene inférieur du Maroc, apports à la phylogeny of the Proboscidea et the ongulés lophodontes". Geodiversitas. 27 (2), 239–333.
Gheerbrant, E., Bouya, B., Amaghzaz, M., 2012. Dental and cranial anatomy of *Eritherium azzouzorum* from the Paleocene of Morocco, earliest known proboscidean mammal. Palaeontographica, A 297, 151–183.
Gheerbrant, E., Amaghzaz, M., Bouya, B., Goussard, F., Letenneur, C., 2014. *Ocepeia* (middle Paleocene of Morocco): the oldest skull of an afrotherian mammal. PLOS One 9, 1–30 (DOI: 10.1371/journal.pone.0089739).
Gheerbrant, E., Cappetta, H., Lapparent de Broin, F. de, Rage, J.-C., and Tabuce, R., 2017. Les faunes de vertébrés marins et terrestres du Paléogène du Bassin d'Ouarzazate, Maroc, in Zouhri, S. ed., Paléontologie des Vertébrés du Maroc: état des connaissances. Mémoire de la Société Géologique de France, v. 180, p. 485–525.
Gheerbrant, E., Schmitt, A., Kocsis, L., 2018. Early African fossils elucidate the origin of embrithopod mammals. – Current Biology 28, 1–7. – https://doi.org/10.1016/j.cub.2018.05.032
Gheerbrant, E., Khaldoune, F., Schmitt, A., Tabuce, R., 2020. Earliest embrithopod mammals (Afrotheria, Tethytheria) from the Early Eocene of Morocco: anatomy, systematics and phylogenetic significance. Journal of Mammal Evolution. https://doi.org/10.1007/s10914-020-09509-6
Goettig, P., Magdolen, V., Brandstetter, H., 2010. Natural and synthetic inhibitors of kallikrein-related peptidases (KLKs). Biochimie 92, 1546–1567.
Hardenbol, J., Thierry, J., Farley, M.B., Jacquin, T., de Graciansky, P.-C., Vail, P.R., 1998. Mesozoic and Cenozoic sequence stratigraphy of European basins. SEPM Spec. Publ. 60, 3–13.
Harrell, T.L., Pérez-Huerta, A., Phillips, G., 2016. Strontium isotope age-dating of fossil shark tooth enameloid from the Upper Cretaceous Strata of Alabama and Mississippi, USA. Cretac. Res. 62, 1–12.
Herbig, H.G., Gregor H.J., 1990. The mangrove-forming palm *Nypa* from the early Paleogene of southern Morocco. Paleoenvironment and paleoclimate. In: Géologie Méditerranéenne. Tome 17, numéro 2, 1990. pp. 123–137.
Herwartz, D., Tütken, T., Münker, C., Jochum, K.P., Stoll, B., Sander, P.M., 2011. Timescales and mechanisms of REE and Hf uptake in fossil bones. Geochim. Cosmochim. Acta 75, 82–105.
Herwartz, D., Tütken, T., Jochum, K.P., Sander, P.M., 2013. Rare earth element systematics of fossil bone revealed by LA-ICPMS analysis. Geochim. Cosmochim. Acta 103, 161–183.
Hodell, D.A., Kamenov, G.D., Hathorne, E.C., Zachos, J.C., Röhl, U., Westerhold, T., 2007. Variations in the strontium isotope composition of seawater during the Paleocene and early Eocene from ODP Leg 208 (Walvis Ridge). Geochem Geophys Geosyst 8:Q09001. doi:10.1029/2007GC001607
Hoppe, K.A., Koch, P.L., Carlson, R.W., Webb, S.D., 1999. Tracking mammoths and mastodons: reconstruction of migratory behavior using strontium isotope ratios. Geology 27, 439–442.
Hyland, G.E., Sheldon, D.N., Cotton, M.J. 2017. Constraining the early Eocene climatic optimum: A terrestrial interhemispheric comparison. GSA Bulletin, 129 (1-2), 244–252.
Ingram, B.L., 1995. High-resolution dating of deep-sea clays using Sr isotopes in fossil fish teeth. Earth and Planetary Science Letters 134, 545–555.
Knidiri, A., Daoudi, L., El Ouahabi, M., Rhouta, B., Rocha, F., Fagel, N., 2014. Palaeogeographic controls on palygorskite occurrence in Maastrichtian-Palaeogene sediments of the western High Atlas and Meseta Basins (Morocco).Clay Minerals 49, 595–608.
Kocsis. L., Vennemann, T.W., Fontignie, D., 2007. Migration of sharks into freshwater systems during the Miocene and implications for Alpine paleoelevation. Geology, 35, 451–454.
Kocsis, L., Osi, A., Vennemann, T.W., Trueman, N.C., Palmer, R.M., 2009. Geochemical study of vertebrate fossils from the Upper Cretaceous (Santonian) Csehbánya formation (Hungary): evidence for a

freshwater habitat of mosasaurs and pycnodont fish. Palaeogeogr. Palaeoclimatol. Palaeoecol. 280, 532–542.
Kocsis, L., Trueman, C.N., Palmer, M., 2010. Protracted diagenetic alteration of REE contents in fossil bioapatites: direct evidence from Lu–Hf isotope systematics. Geochim. Cosmochim. Acta 74, 6077–6092.
Kocsis, L., Ounis, A., Chaabani F., Salah, N.M., 2013. Paleoenvironmental conditions and strontium isotope stratigraphy in the Paleogene Gafsa Basin (Tunisia) deduced from geochemical analyses of phosphatic fossils. International Journal of Earth Sciences 102, 1111–1129.
Kocsis, L., Gheerbrant, E., Mouflih, M., Cappetta, H., Yans, J., Amaghzaz, M., 2014a. Comprehensive stable isotope investigation of marine biogenic apatite from the late Cretaceous-early Eocene phosphate beds of Morocco. – Palaeogeography, Palaeoclimatology, Palaeoecology, 394, 74–88.
Kocsis, L., Ozsvart, P., Becker, D., Ziegler, R., Scherler, L., Codrea, V., 2014b. Orogeny forced terrestrial climate variation during the late Eocene-early Oligocene in Europe. Geology 42, 727–730. http://dx.doi.org/10.1130/g35673.1.
Kocsis, L., Vennemann, T., Ulianov, A., Brunnschweiler, J.M., 2015. Tracing bull shark (Carcharhinus leucas) freshwater habitats in Fiji by chemical and isotopic compositions of their teeth. Environ. Biol. Fish 98 (6), 1609–1622.
Kocsis, L., Gheerbrant, E., Mouflih, M., Cappetta, H., Ulianov, A., Chiaradia, M., Bardet, N., 2016. Gradual changes in upwelled seawater conditions (redox, pH) from the late Cretaceous through early Paleogene at the northwest coast of Africa: Negative Ce anomaly trend recorded in fossil bio-apatite. .Chemical Geology 421, 44–54.
Kohn, M.J., 1996. Predicting animal delta O-18: Accounting for diet and physiological adaptation. Geochim. Cosmochim. Acta 60, 4811–4829. http://dx.doi.org/10.1016/s0016-7037(96)00240-2.
Kohn, M.J., 2010. Carbon isotope compositions of terrestrial C3 plants as indicators of (paleo) ecology and (paleo)climate. National Academy of Sciences Proceedings, v. 107, p. 19691–19695, doi:10.1073/pnas.1004933107.
Kohn, M.J., Cerling, T.E., 2002, Stable isotopes of biological apatite, in Kohn, M.L., et al., eds., Phosphates: Geochemical, geobiological and materials importance: Mineralogical Society of America Reviews in Mineralogy Volume 48, p. 455–488.
Kowal-Linka, M., Jochum, K.P., Surmik, D., 2014. LA-ICP-MS analysis of rare earth elements in marine reptile bones from the Middle Triassic bonebed (Upper Silesia, S Poland): impact of long-lasting diagenesis, and factors controlling the uptake. Chem. Geol. 363, 213–228.
Lécuyer, C., Reynard, B., Grandjean, P., 2004. Rare earth element evolution of Phanerozoic seawater recorded in biogenic apatites. Chem. Geol. 204, 63–102.
Liu, A.G.S.C., Seiffert, E.R., Simons, E.L., 2008. Stable isotope evidence for an amphibious phase in early proboscidean evolution. Proceedings of the National Academy of Sciences 105, 5786–5791. https://doi.org/10.1073/pnas.0800884105
Lucas, J., Prevôt-Lucas, L., 1995. Tethyan phosphates and bioproductites. In: Nairn, A.E. (Ed.), The Ocean Basins and Margins. The Tethys Ocean, vol. 8. Plenum Press, pp. 367–391.
Mahboubi, S., Bocherens, H., Scheffler, M., Benammi, M., Jaeger, J.-J., 2014. Was the Early Eocene proboscidean *Numidotherium koholense* semi-aquatic or terrestrial? Evidence from stable isotopes and bone histology. Comptes Rendus Palevol 13, 501–509. https://doi.org/10.1016/j.crpv.2014.01.002
McArthur, J.M., Howarth, R.J., Shields, G.A., Zhou, Y. 2020. Strontium isotope stratigraphy, Chapter 7. In: Gradstein, F.M., Ogg, J.G., Schmitz, M.D., Ogg, G.M. (Eds.), A Geologic Time Scale, Elsevier B.V., Vol 1 of 2, pp. 211–238.
MacFadden, B.J., Labs-Hochstein, J., Hulbert Jr., R.C., Baskin, J.A., 2007. Revised age of the late Neogene terror bird (Titanis) in North America during the Great American interchange. Geology 35, 123–126.
McLennan, S.M. 1989. Rare earth elements in sedimentary rocks: Influence of provenance and sedimentary processes. In: Lipin RB, McKay AG (Eds.), Geochemistry and Mineralogy of Rare Earth Elements. Review in Mineralogy and Geochemistry vol. 21, pp. 169–200.
Metzger, C.A., Terry, D.O., Grandstaff, D.E., 2004. Effect of paleosol formation on rare earth element signatures in fossil bone. Geology 32, 467–500.
Mohr, B., 1986. Palynologischer Nachweis eines Mangrovenbiotops in der Südatlas-Randzone (Marokko) und seine paläoökologische Bedeuntung. Documenta naturae 33, 20–28.
Mohr, B., Fechner, G., 1986. Eine eozäne Mikroflora (Sporomorphae und Dinoflagellaten-Zysten) aus der Südatlas-Randzone westlich Boumalne du Dadès (Marokko). Berl. Geowiss. Abh. A. 66, 414–481.

906 Mouflih, M., 2015. Les phosphates du Maroc central et du Moyen Atlas (Maastrichtien-Lutétien, Maroc):
907 Sédimentologie, stratigraphie séquentielle, contexte génétique et valorisation. Doctorat d'Etat Es-
908 sciences. Université Cadi Ayyad de Marrakech, Maroc 246 p.
909 Noubhani, A., Cappetta, H., 1997. Les Orectolobiformes, Carcharhiniformes et Myliobatiformes
910 (Elasmobranchii, Neoselachii) des bassins à phosphate du Maroc (Maastrichtien-Lutétien basal).
911 Systématique, biostratigraphie, évolution et dynamique des faunes. Palaeo-Ichthyologica 8, 1–327.
912 Office Chérifien des Phosphates, 1989. The phosphates basins of Morocco. In: Notholt, A.J.G., Sheldon, R.P.,
913 Davidson, D.F. (Eds.), Phosphates Deposits of the World, Phosphate Rock Resources. Cambridge
914 University Press, Cambridge, pp. 301–311.
915 Ollivier-Pierre, M.F., 1982. La microflore du Paléocène et de l'Eocène des series phosphatées des ganntour
916 (Maroc). Sci. Géol. Bull. 35 (3), 117–127.
917 Pearce, N.J.G., Perkins, W.T., Westgate, J.A., Gorton, M.P., Jackson, S.E., Neal, C.R., Chenery, S.P., 1997. A
918 compilation of new and published major and trace element data for NIST SRM 610 and NIST SRM 612
919 glass reference materials. Geostand. Geoanal. Res. 21, 115–144.
920 Pearson, P.N., Palmer, M.R., 2000. Atmospheric carbon dioxide concentrations over the past 60 million years.
921 Nature 406, 695–699.
922 Pereda Suberbiola, X., Bardet, N., Iarochène, M., Bouya, B., Amaghzaz, M., 2004. The first record of a sauropod
923 dinosaur from the Late Cretaceous phosphates of Morocco. Journal of African Earth Sciences 40, 81–88.
924 Picard, P., Lécuyer, C., Barrat, J.-A., Garcia, J.-P., Dromart, G., Sheppard, S.M.F., 2002. Rare earth element
925 contents of Jurassic fish and reptile teeth and their potential relation to seawater composition (Anglo-
926 Paris Basin, France and England). Chem. Geol.186,1–16.
927 Pin, C., Briot, D., Bassin, C., Poitrasson, F., 1994. Concomitant separation of strontium and samarium–
928 neodymium for isotopic analysis in silicate samples, based on specific extraction chromatography. Anal.
929 Chim. Acta 298, 209–217.
930 Rauscher, R., 1985. Les dinokystes, des outils stratigraphiques pour les séries phosphatées. Application aux
931 phosphorides du Maroc. Sci. Géol. Bull. 77, 69–74.
932 Reynard, B., Balter, V., 2014. Trace elements and their isotopes in bones and teeth: Diet, environments,
933 diagenesis, and dating of archeological and paleontological samples. Palaeogeogr. Palaeoclimatol.
934 Palaeoecol. 416, 4–16
935 Reynard, B., Lécuyer, C., Grandjean, P., 1999. Crystal–chemical controls on rare earth element concentrations
936 in fossil biogenic apatites and implications for paleoenviromental reconstructions. Chem. Geol. 155,
937 233–241.
938 Schubert, A.B, Jahren, A.H., 2012. The effect of atmospheric CO2 concentration on carbon isotope
939 fractionation in C3 land plants. Geochimica et Cosmochimica Acta 96, 29–43.
940 Secord, R., Wing, L.S., Chew, A., 2008. Stable Isotopes in Early Eocene Mammals as Indicators of Forest Canopy
941 Structure and Resource Partitioning. Paleobiology, 34(2),. 282–300.
942 Shields, G.A., Webb, G.E., 2004. Has the REE composition of seawater changed over geologic time. Chem. Geol.
943 204, 103–107.
944 Simmer, J.P., Hu, Y., Lertlam, R., Yamakoshi, Y., Hu, J.C.C., 2009. Hypomaturation enamel defects in Klk4
945 knockout/LacZ knockin mice. J Biol Chem 284, 19110–19121.
946 Snedden, J.W., Liu, C., 2010. A compilation of Phanerozoic sea level change, coastal onlaps, and recommended
947 sequence designations: AAPG Search and Discovery article 40594,
948 http://www.searchanddiscovery.net/documents/2010/40594snedden/ndx_snedden.pdf (accessed
949 October 2020)
950 Soncini, M.-J., 1990. Palynologie des phosphates des Oulad Abdoun (Maroc). Biostratigraphie et
951 environnements de lab phosphatogenèse dans le cadre de la crise Crétacé/Tertiaire. Université Louis
952 Pasteur, Strasbourg, p. 243. Ph.D. thesis.
953 Staron, R.M., Grandstaff, B.S., Gallagher, W.B., Grandstaff, D.E., 2001. REE signatures in vertebrate fossils from
954 Sewell, NJ: implications for location of the K–T boundary. Palaios 16, 255–265.
955 Suarez, C.A., Macpherson, G.L., González, L.A., Grandstaff, D.E., 2010. Heterogeneous rare earth element (REE)
956 patterns and concentrations in a fossil bone: implications for the use of REE in vertebrate taphonomy
957 and fossilisation history. Geochim. Cosmochim. Acta 74, 2970–2988.
958 Trueman, C.N., Tuross, N., 2002. Trace elements in recent and fossil bone apatite. In: Kohn, M.J., Rakovan, J.,
959 Hughes, J.M. (Eds.), Phosphates: Geochemical, Geobiological, and Materials Importance. Review in
960 Mineralogy and Geochemistry vol. 48, pp. 489–521.
961 Trueman, C.N., Benton, M.J., Palmer, M.R., 2003. Geochemical taphonomy of shallow marine vertebrate
962 assemblages. Palaeogeogr. Palaeoclimatol. Palaeoecol. 197, 151–169.

963 Trueman, C.N., Kocsis, L., Palmer, M.R., Dewdney, C., 2011. Fractionation of rare earth elements within bone
964 mineral: a natural cation exchange system. Palaeogeogr. Palaeoclimatol. Palaeoecol. 310, 124–132.
965 Tütken, T., Vennemann, W.T., Janz, H., Heizmann, E.P.J. 2006. Palaeoenvironment and palaeoclimate of the
966 Middle Miocene lake in the Steinheim basin, SW Germany: A reconstruction from C, O, and Sr isotopes
967 of fossil remains. Palaeogeography, Palaeoclimatology, Palaeoecology 241, 457–491.
968 Tütken, T., Vennemann, T.W., Pfretzschner, H.-U., 2008. Early diagenesis of bone and tooth apatite in fluvial
969 and marine settings: constraints from combined oxygen isotope, nitrogen and REE analysis.
970 Palaeogeogr. Palaeoclimatol. Palaeoecol. 266, 254–268.
971 Tütken, T., 2014. Isotope compositions (C, O, Sr, Nd) of vertebrate fossils from the Middle Eocene oil shale of
972 Messel, Germany: Implications for their taphonomy and palaeoenvironment. Palaeogeography,
973 Palaeoclimatology, Palaeoecology 416, 92–109
974 Vail, P.R., Audemard, E., Bowman, S.A., Eisner, P.N., Perez-Crus, C., 1991. The stratigraphic signatures of
975 tectonics, eustasy and sedimentology–an overview, in Einsele, G., Ricken, W., and Seilacher, A., eds.,
976 Cycles and events in stratigraphy: Springer-Verlag, Berlin, p. 617–659.
977 van der Meer, D.G., van den Berg van Saparoea, A.P., van Hinsbergen, D., van de Weg, R., Godderis, Y., Le Hir,
978 G., Donnadieu, Y., 2017. Reconstructing first-order changes in sea level during the Phanerozoic and
979 Neoproterozoic using strontium isotopes: Gondwana Research 44, 22–34.
980 van Hinsbergen, D.J.J., de Groot, L.V., van Schaik, S.J., Spakman, W., Bijl, P.K., Sluijs,A., Langereis, C.G.,
981 Brinkhuis, H., 2015. A paleolatitude calculator for paleoclimate studies. PLoS ONE 10, e0126946–21.
982 http://dx.doi.org/10.1371/journal.pone.0126946
983 Wei, L., Yan, C., Ye, B., Guo, X., 2008. Effects of Salinity on Leaf $\delta^{13}C$ in Three Dominant Mangrove Species
984 along Salinity Gradients in an Estuarine Wetland, Southeast China. J. of Coastal Research, 241, 267–272.
985 White, W.M., 1998. The Ocean as a Chemical system. Geochemistry, an on-line textbook, vol. 15. pp 645–701.
986 Yans, J., Amaghzaz, M., Bouya, B., Cappetta, H., Iacumin, P., Kocsis, L., Mouflih, M., Selloum, O., Sen, S.,
987 Storme1, J.-Y., Gheerbrant, E., 2014. First carbon isotope chemostratigraphy of the Ouled Abdoun
988 phosphate Basin, Morocco; implications for dating and evolution of earliest African placental mammals.
989 Gondwana Research 25, 257–269.
990 Zazzo, A., Lécuyer, C., Mariotti, A., 2004. Experimentally-controlled carbon and oxygen isotope exchange
991 between bioapatites and water under inorganic and microbially-mediated conditions: Geochimica et
992 Cosmochimica Acta 68, 1–12, doi:10.1016/S0016 -7037 (03) 00278-3.
993 Žigaitė, Ž., Fadel, A., Blom, H., Pérez-Huerta, A., Jeffries, T., Märss, T., Ahlberg, P.E., 2016. Palaeoenvironments
994 revealed from rare earth element systematics in vertebrate bioapatite from the Lower Devonian of
995 Svalbard. In: In: Melchin, M., Jisou, J. (Eds.), Canadian Journal of Earth Sciences, vol. 53. pp. 788–794 8.
996 Žigaitė, Ž., Qvarnström, M., Bancroft, A., Pérez-Huerta, A., Blom, H., Ahlberg, P.E., 2020. Trace and rare earth
997 element compositions of Silurian conodonts from the Vesiku Bone Bed: Histological and
998 palaeoenvironmental implications. Palaeogeography, Palaeoclimatology, Palaeoecology 549 109449.
999
1000

Figure captions

Figure 1 (a) The origins of the fossils from the Ouled Abdoun Basin in Morocco studied here. Quarries in the Sidi Daoui and Sidi Chennane (grey boxes) are the regions from which most of the remains were reported. The background geochemical data are also derived here (see Figure 5). **(b)** Generalized stratigraphic log of the Ouled Abdoun Basin. Note the major bone beds and the mammal-bearing layers, however, many specimens were obtained without an exact stratigraphic position. Abbreviation: BCbb – big coprolite bone bed. **c)** Examples of some of the mammals found in the Ouled Abdoun phosphate series, successively from lowermost to uppermost levels: *Eritherium azzouzorum* (skull rostrum with teeth in ventral view; Gheerbrant, 2009), the earliest known proboscidean, lower bone bed of bed IIa, Selandian; *Phosphatherium escuilliei* (skull in ventral view; Gheerbrant et al., 2005), early proboscidean, intercalary beds II/I, early Ypresian; *Daouitherium rebouli* (lower jaw ML 20269987 in lateral view), the first large proboscidean (Gheerbrant et al., 2002), upper phosphates levels (bed 0?), middle Ypresian; *Stylolophus major* (maxillary with teeth; Gheerbrant et al., 2018, 2020), earliest known embrithopod with *S. minor*, uppermost phosphates levels, bed 0 or sillons, middle Ypresian.

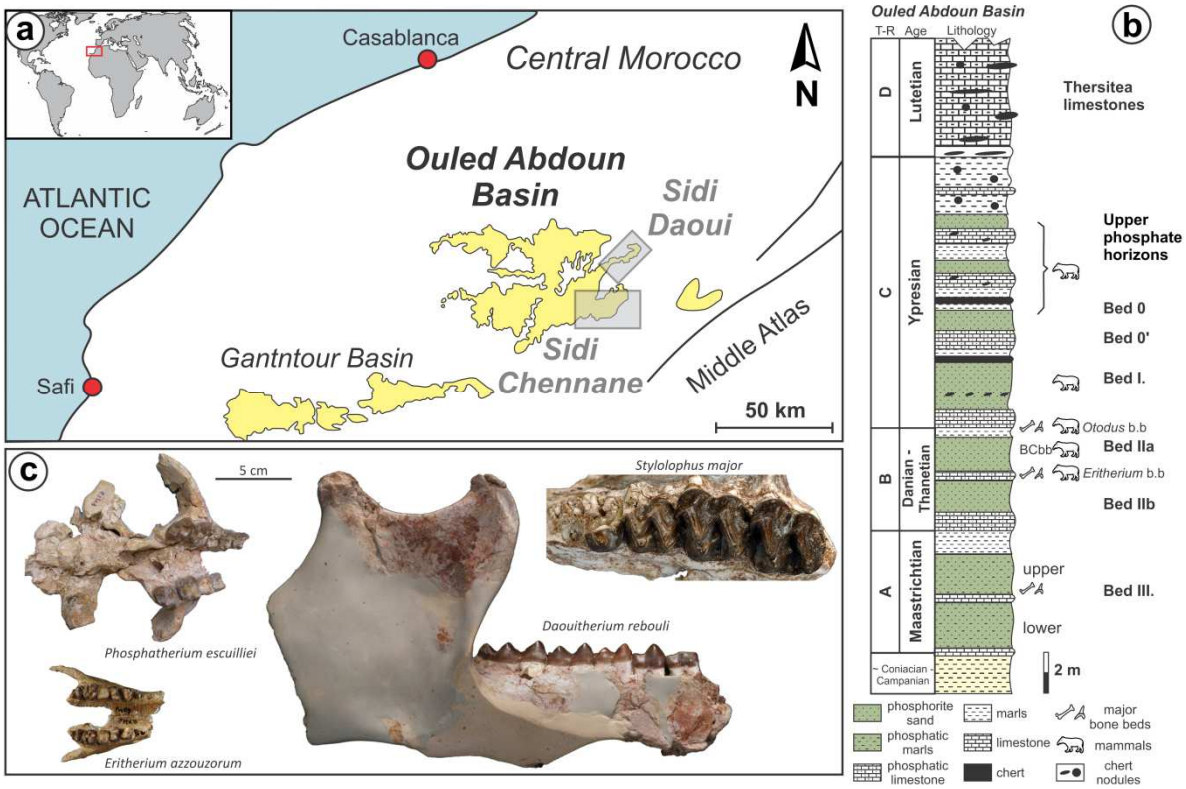

1019 **Figure 2** Major element compositions of selected mammals, shark teeth and coprolites from
1020 the Ouled Abdoun Basin.

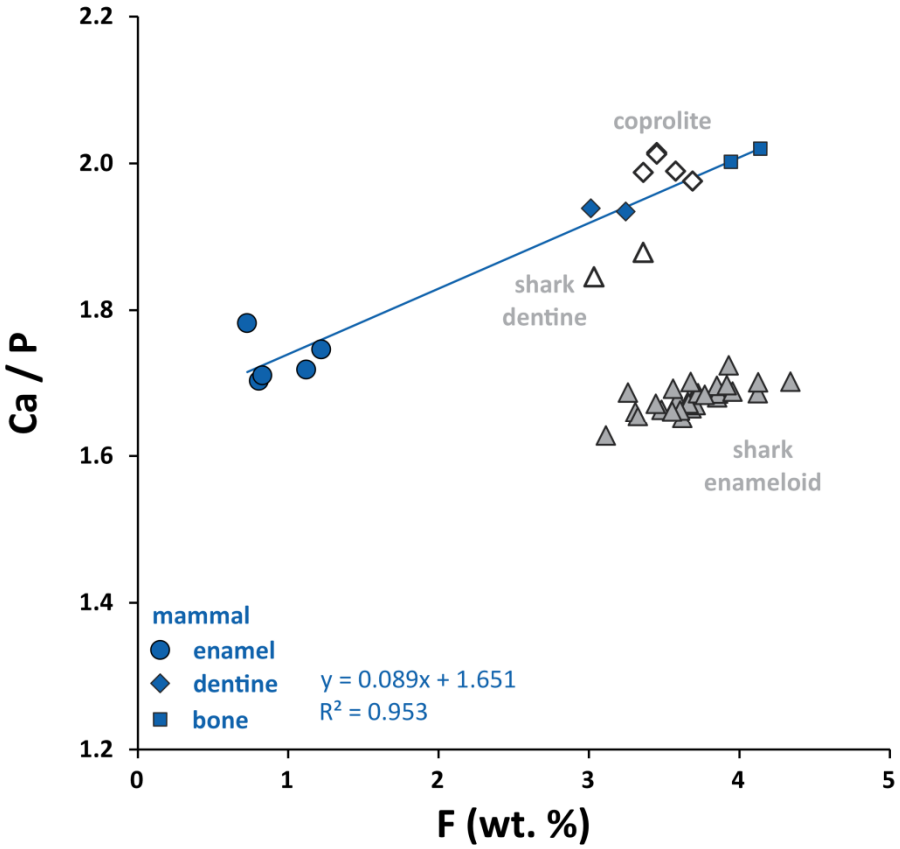

1021

1022

Figure 3 Boxplots of selected trace elements. The label "Mammal" reflects data directly analyzed from the mammal remains (tooth enamel, dentine, and bone), while the label "Matrix" refers to data from fossils derived from the sediment matrix (shark tooth enameloid, dentine, and coprolite) related to the mammals. Student's t-tests were performed to check for statistical differences among these groups (Supplementary Material Table-4). Note that, Sr content in shark tooth enameloid and Ba content in mammal enamel are significantly higher than in the rest of the materials (marked red). Zinc concentration is the highest in enamel and enameloid, and both differ significantly from the coprolite data, whereas shark tooth enameloid is also statistically dissimilar from the dentine and bone data. The REE concentration is the lowest in the enamel/enameloid with significant differences from the other materials (marked red). Distribution of U content among the materials mimics more or less that of the REEs, however with various significances among the different groups (see Supplementary Material Table-4). The Ce/Ce* data yielded no statistical differences among the groups.

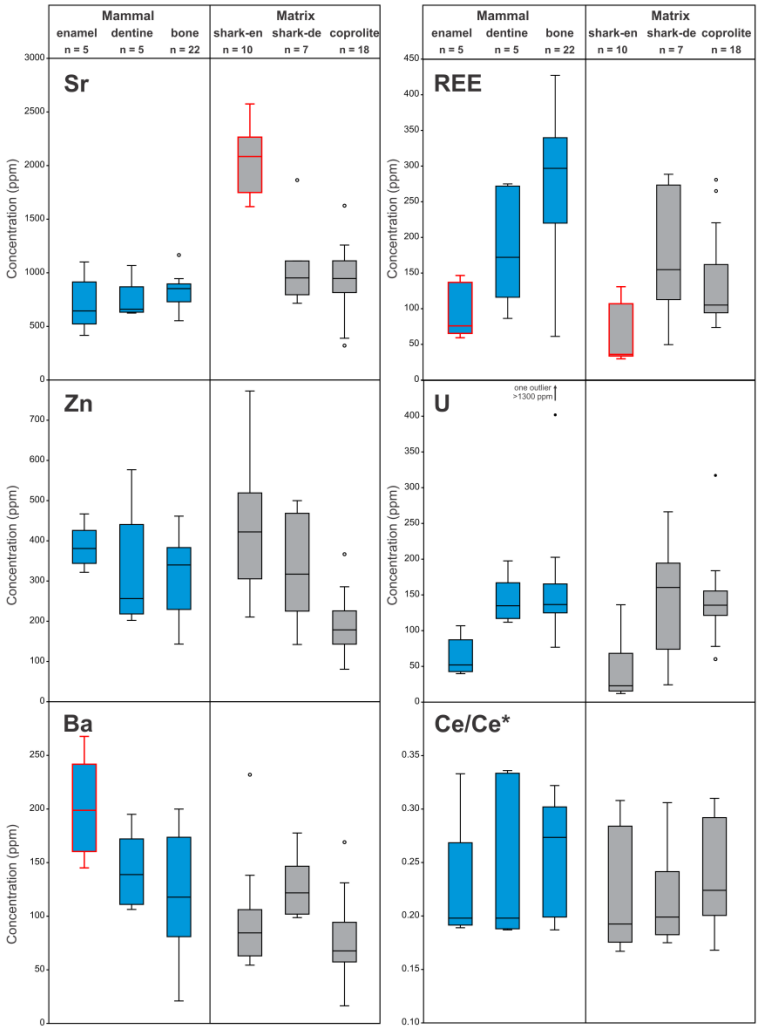

Figure 4 Ce/Ce* and Pr/Pr* variations among the samples. **(a)** Background data from the Ouled Abdoun Basin derived from fish teeth, bones and coprolites (Kocsis et al., 2016). Note the time-wise trending of the samples in the basin. The few overlapping samples show meaningful stratigraphic separation, see Figure 5. **(b-d)** Comparisons of the Paleocene and Eocene background data with the various mammal groups being investigated. Note that the samples are better separated by Ce/Ce* than by Pr/Pr*. Inset figures display examples of PAAS normalized REE patterns. Note the similarities in the REE distributions among the various materials (a) and taxa (b-d).

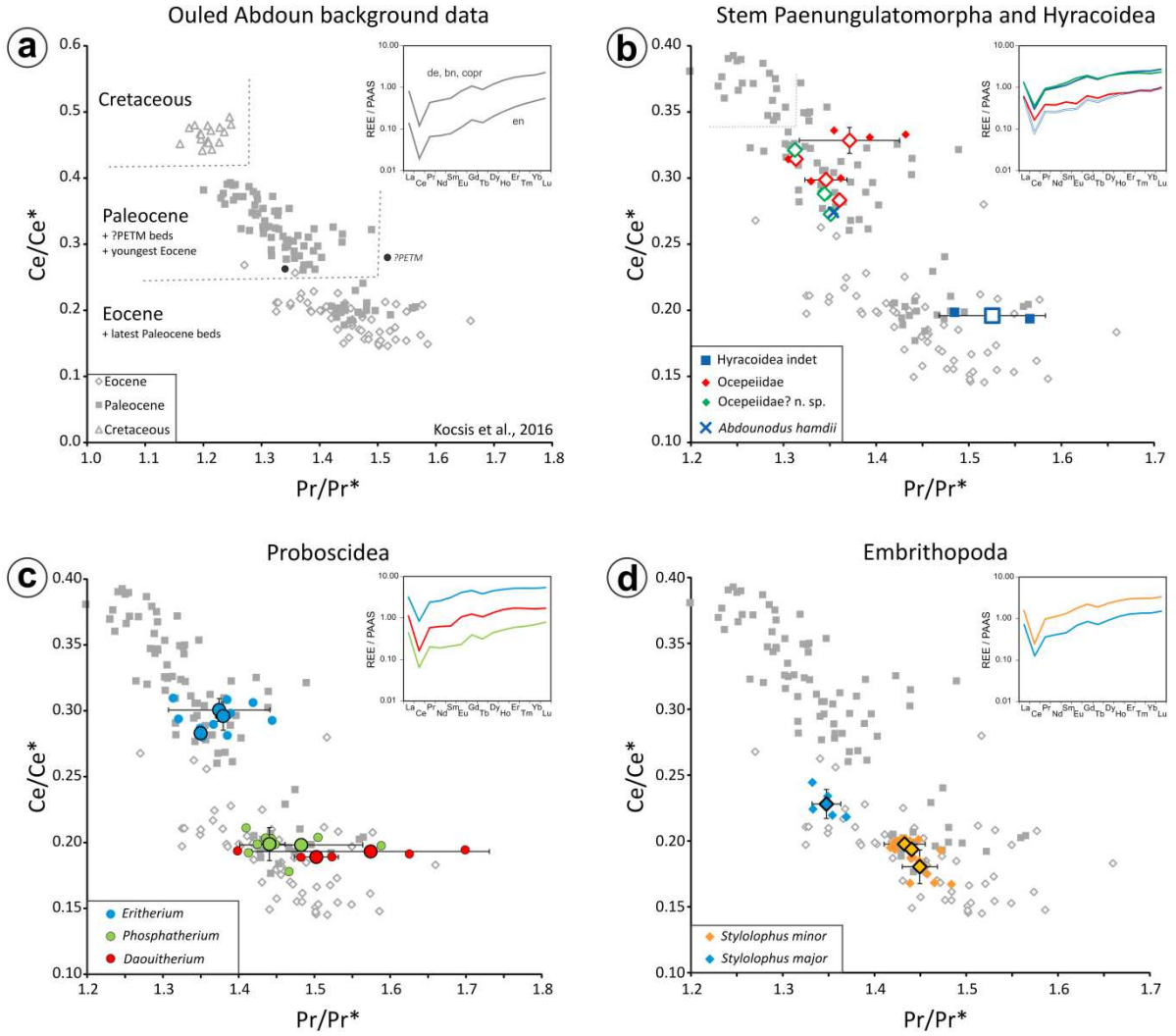

Figure 5 Stratigraphic variation of Ce/Ce* in the Ouled Abdoun Basin based on Kocsis et al. (2016) and new data provided in Supplementary Material Table-1. Note that the data are derived from two quarrying areas: Sidi Daoui and Sidi Chennane. Based on the variation of the Ce/Ce* values the section is divided into 10 horizons (see text and Table 3). Int. III/II and Int. II/I refer to intercalary beds respectively between Bed III and II, and, Bed II and I. Note that the Ce/Ce* data for the few mammal remains (*S. minor* and *E. azzouzorum*) with known stratigraphic origins fit well with the background dataset.

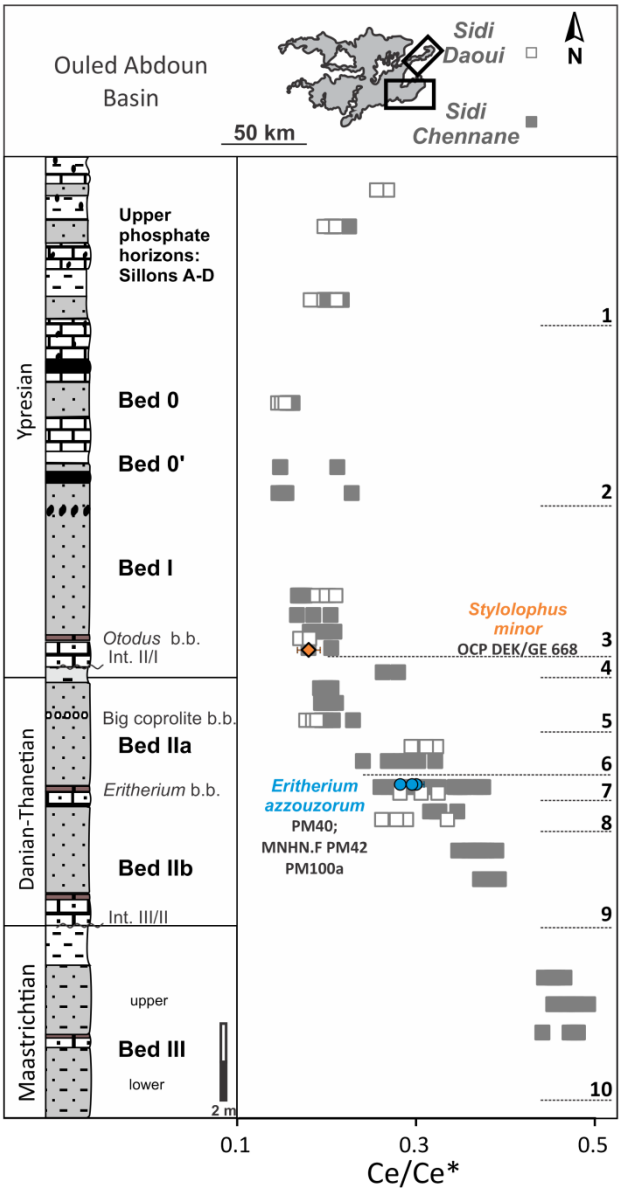

Figure 6 Stratigraphic origins of the mammal remains from the Ouled Abdoun Basin studied here, inferred from comparisons of their mean Ce/Ce* ratios with the average stratigraphic values of the 10 chemostratigraphic horizons (see also Table 3). Note that the thickness of the lines reflects different probabilities. Where only one specimen was analyzed a dashed line is used. In some cases, the composition of the sediment matrix and the selachian fauna (i.e., sharks and rays) give further clue about the possible provenance. The vertical extension of the bar across several levels for some species does not necessarily indicate a wide stratigraphic range, but the best probability of their stratigraphic origin following the Ce/Ce* chemostratigraphy. However, when other factors (e.g., the sedimentary matrix and related fauna) are considered, their provenance can be reduced further, as indicated by the grey background. The yellow background is used for those fossils whose stratigraphic origin was known previously (see Figure 5).

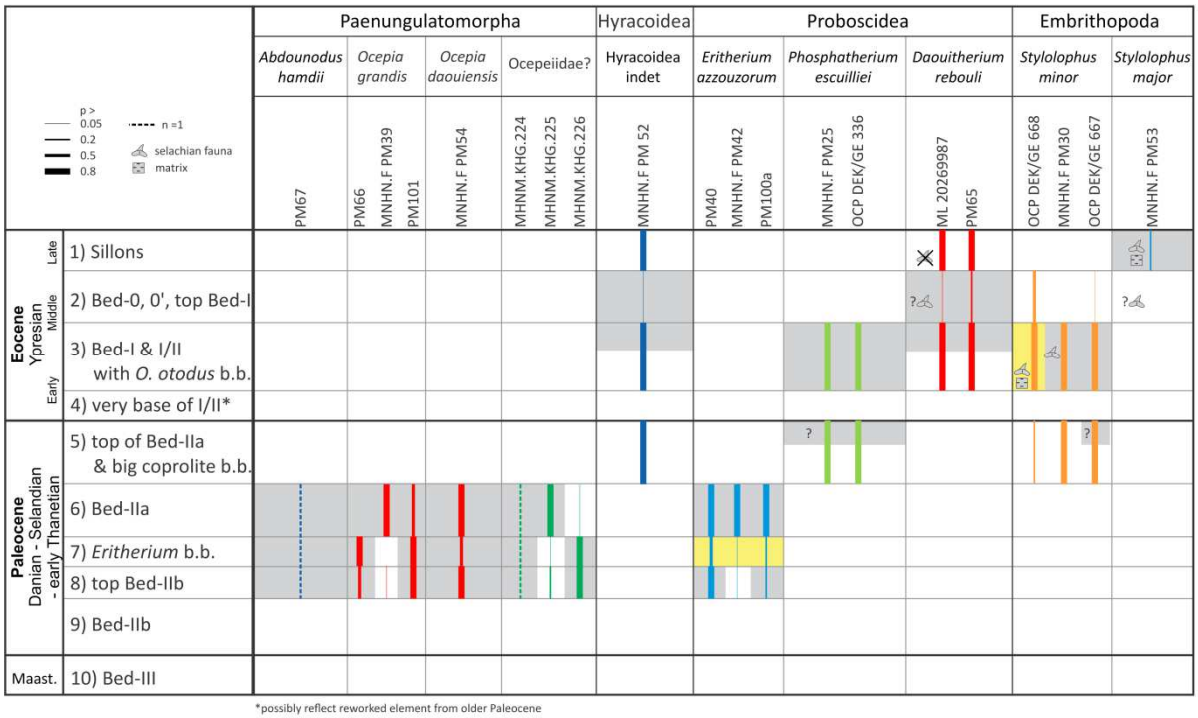

*possibly reflect reworked element from older Paleocene

Figure 7 Strontium isotope variation and its comparison with the global Sr-evolution curve (McArthur et al., 2020). Dashed lines represent the 95% confidence limits. **(a)** Mammal samples with circles. Note that these data are well above the open ocean Sr-evolution curve and the $^{87}Sr/^{86}Sr$ ratios decrease from enamel to bone. The enamel end-members could reflect *in-vivo* Sr ratios, while the dentine and bone show various interactions with seawater. Triangles are individual shark tooth enameloid analyses from the Ouled Abdoun (OA) and Ganntour (GB) basins. The data are plotted according to stratigraphic occurrence and predicted ages (see Supplementary material Table-5). **(b)** Layer averaged $^{87}Sr/^{86}Sr$ ratios of shark tooth enameloid from the previous graph for the phosphate series (triangles) and foraminifera Sr-isotope data from Hodell et al. (2007). The average data are plotted according to ages derived from McArthur et al. (2020). Note that the latest Cretaceous and most of the Paleocene are above the Sr-evolution curve.

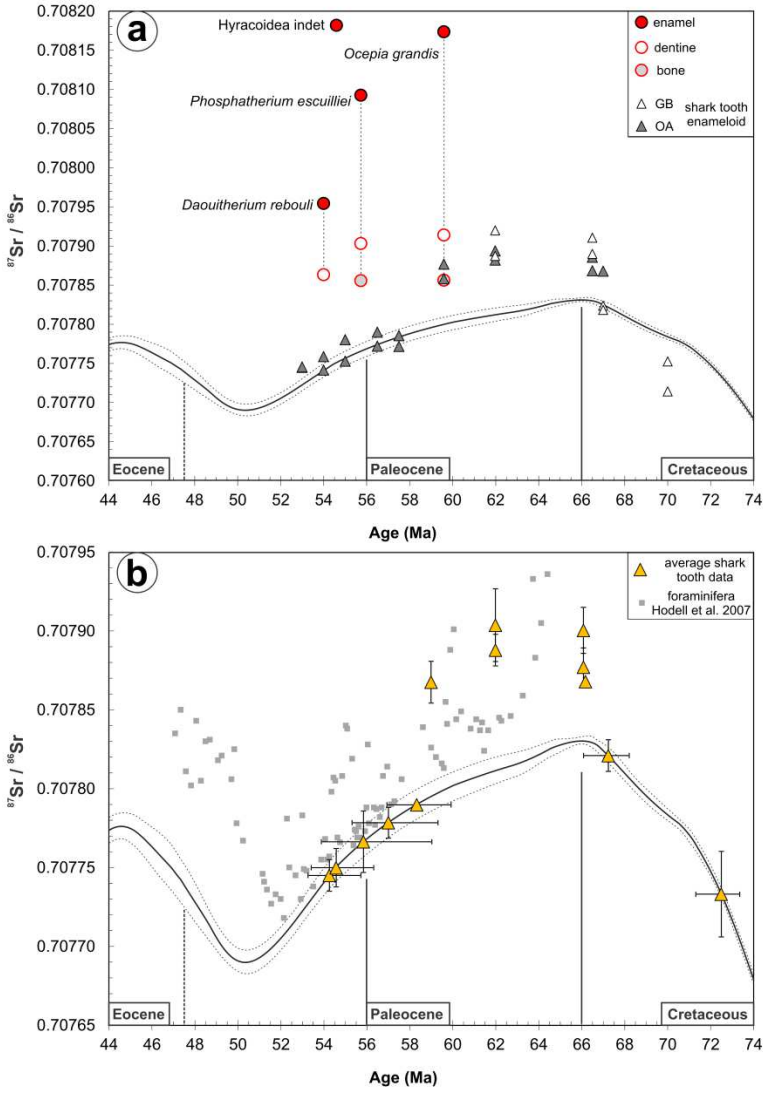

Figure 8 Stable isotope compositions of selected mammal taxa and related ecological and environmental parameters. **(a)** Oxygen isotopic composition of phosphate. The derived isotopic composition of the ingested water and the mean annual temperature (MAT) are calculated based on Amiot et al. (2004). **(b)** Carbon isotopic composition of the structural carbonate and the calculated plant diet isotopic composition after Kohn and Cerling (2002). Note the increasing trend from enamel to bone, indicating an alteration in the presence of seawater.

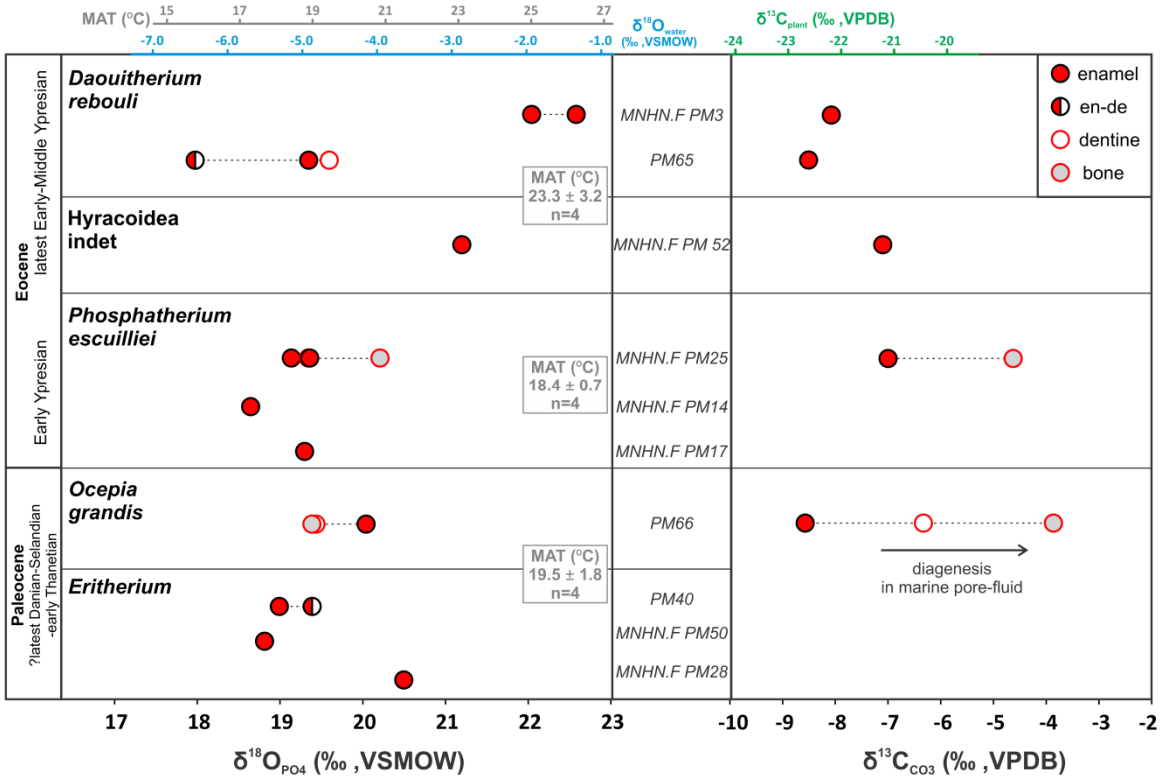

Table captions

Table 1 The mammal remains investigated, and related analyses. Note the uncertain stratigraphic origin, column Locality/Layers, indicated by question marks. Abbreviations: en – enamel, de – dentine, th – tooth, sh – shark tooth, ra – ray tooth, copr – coprolite, pel – pellets.

						ICP-REE							
Inventory No.	Order	Family	Species	Locality / Layer	Age	specimen	matrix	No.	$\delta^{18}O_{PO4}$	$\delta^{13}C$-$\delta^{18}O_{CO3}$	$^{87}Sr/^{86}Sr$	EMPA	References
MNHN.F PM3	Proboscidea	Numidotheriidae?	*Daouitherium rebouli*	above CI?	Ypresian	-	-	-	+	+			Gheerbrant et al., 2012
PM65	Proboscidea	Numidotheriidae?	*Daouitherium cf. rebouli*	above CI?	Ypresian	en, de	-	2	+	+	+	+	Gheerbrant et al., 2012
ML 20269987	Proboscidea	Numidotheriidae?	*Daouitherium rebouli*	CO? (selachians)	Ypresian	-	sh, copr	3					
MNHN.F PM 52	Hyracoidea	Indet	Hyracoidea indet	?	?Ypresian	en, de	-	2	+	+	+	+	unpublished
MNHN.F PM53	Embrithopoda	Stylolophidae	*Stylolophus major*	sillons?	Ypresian	en & de	sh (en-de), copr	2 + 3					Gheerbrant et al., in press
MNHN.F PM30	Embrithopoda	Stylolophidae	*Stylolophus minor*	intercalary II/I?	Ypresian	bn	sh, copr	3 + 2					Gheerbrant et al., 2018
OCP DEK/GE 667	Embrithopoda	Stylolophidae	*Stylolophus minor*	intercalary II/I?	Ypresian	bn	copr	3 + 2					Gheerbrant et al., 2018
OCP DEK/GE 668	Embrithopoda	Stylolophidae	*Stylolophus minor*	*Otodus* bonebed, intercalary II/I	Ypresian	bn, th	sh (en-de), copr	2 + 6					Gheerbrant et al., 2018
MNHN.F PM25	Proboscidea	Phosphatheriidae	*Phosphatherium escuilliei*	?	Ypresian	en, de, bn	sh	3 + 1	+	+	+	+	Gheerbrant et al., 2005
OCP DEK/GE 336	Proboscidea	Phosphatheriidae	*Phosphatherium escuilliei*	?	Ypresian	-	sh (en-de), ra, copr	4					Gheerbrant et al., 2005
MNHN.F PM14	Proboscidea	Phosphatheriidae	*Phosphatherium escuilliei*	intercalary II/I	Ypresian	-	-	-	+				Gheerbrant et al., 2005
MNHN.F PM17	Proboscidea	Phosphatheriidae	*Phosphatherium escuilliei*	intercalary II/I	Ypresian	-	-	-	+				Gheerbrant et al., 2005
PM67	Paenungulatomorpha	Indet	*Abdounodus hamdii*	?	Paleocene	bn	-	1					Gheerbrant 2010
PM66	Paenungulatomorpha	Ocepeiidae	*Ocepia grandis*	?CIIa, ?big coprolite bone bed	Paleocene	en, de, bn	-	4	+	+	+	+	Gheerbrant et al., 2014
MNHN.F PM39	Paenungulatomorpha	Ocepeiidae	*Ocepia grandis*	?	Paleocene	bn	-	2					Gheerbrant et al., 2014
PM101	Paenungulatomorpha	Ocepeiidae	*Ocepia grandis*	?	Paleocene	bn	-	2					unpublished
MNHN.F PM54	Paenungulatomorpha	Ocepeiidae	*O. daouiensis*	?	Paleocene		copr, pell	2					Gheerbrant et al., 2014
MHNM.KHG.224	Paenungulatomorpha	Ocepeiidae?	n. sp.	?	Paleocene	bn	-	1					unpublished
MHNM.KHG.225	Paenungulatomorpha	Ocepeiidae?	n. sp.	?	Paleocene	bn	-	2					unpublished
MHNM.KHG.226	Paenungulatomorpha	Ocepeiidae?	n. sp.	?	Paleocene	bn	-	2					unpublished
PM40	Proboscidea	indet.	*Eritherium azzouzorum*	*Eritherium* bone bed	Paleocene	-	sh (en-de), copr	4	+				Gheerbrant et al., 2012
MNHN.F PM50	Proboscidea	indet.	*Eritherium azzouzorum* (juvenile)	*Eritherium* bone bed	Paleocene	-	-	-	+				Gheerbrant et al., 2012
OCP DEK/GE 498	Proboscidea	indet.	cf. *Eritherium* sp.	*Eritherium* bone bed	Paleocene	-	-	-					unpublished
MNHN.F PM28	Proboscidea	indet.	*Eritherium azzouzorum*	*Eritherium* bone bed	Paleocene	-	-	-	+				Gheerbrant et al., 2012
MNHN.F PM42	Proboscidea	indet.	*Eritherium azzouzorum*	*Eritherium* bone bed	Paleocene	-	copr	3					Gheerbrant et al., 2012
PM100a	Proboscidea	indet.	*Eritherium azzouzorum*	*Eritherium* bone bed	Paleocene	bn	sh (en), copr	1 + 4					unpublished

Table 2 Major element, Sr-isotope ratios, and stable oxygen and carbon isotopic compositions of selected mammal specimens. Abbreviations: en – enamel, de – dentine, en-de – enamel dentine transition.

No.	Species	Material		CaO (wt%)	P_2O_5 (wt%)	F (wt%)	Ca/P	n	$^{87}Sr/^{86}Sr$	1SE x10^{-6}	Ma	$\delta^{18}O_{PO4}$ VSMOW	std.	Specimen average	std.	Taxon average	std.	$\delta^{13}C$ VPDB	std.	$\delta^{18}O$ VPDB	$\delta^{18}O$ VSMOW	std.	Yield (%)
MNHN.F PM3	*Daouitherium rebouli*	right m3	en									22.0	0.1										
			en									22.6	0.2	22.3	0.4								
PM65	*Daouitherium rebouli*	dP2-4 and M1	en	51.7	36.7	0.73	1.78	3	0.707954	3	54	19.3	0.1					-8.1	0.1	-4.2	26.6	0.2	3.9
			en-de	50.2	37.0	1.12	1.72	1				18.0	0.1					-8.5	0.1	-5.0	25.8	0.1	6.5
			de	45.1	29.5	3.01	1.94	3	0.707863	3	54	19.6	0.2	19.0	0.9	20.6	2.4						
MNHN.F PM 52	Hyracoidea indet	m3	en	50.3	37.2	0.83	1.71	3	0.708182	3	58	21.2	0.1	21.2	0.3	21.2		-7.1	0.1	-3.7	27.1	0.1	6.5
MNHN.F PM25	*Phosphatherium escuilliei*	right p3	en	52.1	38.7	0.81	1.70	3	0.708093	5	56.5	19.4	0.1					-7.0	0.1	-4.4	26.4	0.1	5.9
			de	49.4	31.2	3.95	2.00	2	0.707903	3	56.5	19.3	0.2										
		right m1	en									19.1	0.1										
		jaw frg.	bone	50.0	31.3	4.14	2.02	2	0.707856	3	56.5	20.2	0.0	19.5	0.5			-4.6	0.1	-5.1	25.7	0.0	7.0
MNHN.F PM14	*Phosphatherium escuillici*	m3	en									18.6	0.2	18.6	0.3								
MNHN.F PM17	*Phosphatherium escuilliei*	right M2	en									19.3	0.3	19.3	0.3	19.2	0.5						
PM66	*Ocepia grandis*	tooth fragment	en	50.3	36.5	1.22	1.75	2	0.708174	3	58	20.0	0.0					-8.6	0.1	-4.8	26.0	0.1	6.4
			de	48.9	32.0	3.25	1.93	2	0.707914	4	58	19.4	0.0					-6.3	0.1	-5.6	25.1	0.0	5.8
		bone fragment	bone						0.707856	3	58	19.4	0.3	19.6	0.4	19.6	0.4	-3.9	0.1	-5.6	25.2	0.0	6.8
PM40	*Eritherium*	m1	en									19.0											
			en-de									19.4	0.2	19.2	0.3								
MNHN.F PM50	*Eritherium*	p2	en									18.8	0.3	18.8	0.3								
MNHN.F PM28	*Eritherium*		en									20.5	0.1	20.5	0.3	19.5	0.9						

Table 3 Tukey's pairwise tests comparing the samples separately with designated horizons. In the case of Eocene mammals Horizons 1-5, while for the Paleocene taxa Horizons 5-10 were used. Note that only the probability values are listed. Layers with highlighted values could be considered as a possible provenance for the given mammal fossils, while the strikethrough numbers indicate invalid scenarios. See also text and Figure 6.

Eocene mammals

Tukey's pairwise test p (same) relative to the horizons (1-5)				MNHN.F PM53 *S. major*	OCP DEK/GE 668 *S. minor*	MNHN.F PM30 *S. minor*	OCP DEK/GE 667 *S. minor*	MNHN.F PM25 *P. escuilliei*	OCP DEK/GE 336 *P. escuilliei*	ML 20269987 *D. rebouli*	PM65 *D. rebouli*	MNHN.F PM 52 Hyracoidea indet
H.	Age	Beds	n	5	8	5	5	4	5	3	2	2
1	late Ypresian	Sillons	22	0.30	~~0.19~~	~~0.98~~	~~0.90~~	~~0.99~~	~~0.99~~	0.92	0.81	0.98
2	latest Early - Middle Ypresian	Bed 0-0' & Top Bed I	14	< 0.05	0.56	< 0.05	0.07	< 0.05	< 0.05	0.12	0.34	0.12
3	early Ypresian	Bed-I & I/II	23	< 0.05	0.99	0.93	0.99	0.92	0.90	1.00	1.00	0.98
4	?PETM	base I/II	2	< 0.05	< 0.05	< 0.05	< 0.05	< 0.05	< 0.05	< 0.05	< 0.05	< 0.05
5	late Thanetian	Top Bed IIa & Big Copr Bed	18	~~0.10~~	0.47	1.00	1.00	1.00	1.00	~~1.00~~	~~0.97~~	1.00

Paleocene mammals

Tukey's pairwise test p (same) relative to the horizons (5-10)				PM40 *Eritherium azzouzorum*	MNHN.F PM42 *Eritherium azzouzorum*	PM100a *Eritherium*	PM66 *Ocepia grandis*	MNHN.F PM39 *Ocepia grandis*	PM101 *Ocepia grandis*	MNHN.F PM54 *O. daouiensis*	MHNM.KHG.225 *Ocepeiidae?*	MHNM.KHG.226 *Ocepeiidae?*
H.	age	Beds	n	4	3	5	4	2	2	2	2	2
5	late Thanetian	Top Bed-IIa & Big Copr Bed	18	< 0.05	< 0.05	< 0.05	< 0.05	< 0.05	< 0.05	< 0.05	< 0.05	< 0.05
6	Selandian-early Thanetian	Bed-IIa	10	0.99	0.96	1.00	< 0.05	0.98	0.53	1.00	1.00	0.19
7	Selandian-early Thanetian	Eritherium bone bed	30	0.49	< 0.05	0.17	0.96	< 0.05	1.00	0.59	0.11	1.00
8	Early Selandian-latest Danian	top Bed-IIb	11	0.85	0.06	0.49	0.73	0.14	1.00	0.87	0.30	0.99
9	earliest Selandian-late Danian	Bed-IIb	15	< 0.05	< 0.05	< 0.05	< 0.05	< 0.05	< 0.05	< 0.05	< 0.05	< 0.05
10	latest Maastrichtian	Bed-III	18	< 0.05	< 0.05	< 0.05	< 0.05	< 0.05	< 0.05	< 0.05	< 0.05	< 0.05

Table 4 Tukey's pairwise tests among the Eocene and Paleocene mammal samples. Note that *S. major* is completely different from the rest of the Eocene fossils, while among the Paleocene samples some of the Ocepeiidae spp. (e.g., PM66 & MHNM.KHG.226) are somewhat different from the rest.

Eocene mammals

Tukey's pairwise test Q / p (same)	MNHN.F PM53 *S. major*	OCP DEK/GE 668 *S. minor*	MNHN.F PM30 *S. minor*	OCP DEK/GE 667 *S. minor*	MNHN.F PM25 *P. escuilliei*	OCP DEK/GE 336 *P. escuilliei*	ML 20269987 *D. rebouli*	PM65 *D. rebouli*	MNHN.F PM 52 Hyracoidea indet
S. major		*< 0.05*	*< 0.05*	*< 0.05*	*< 0.05*	*< 0.05*	*< 0.05*	*< 0.05*	*< 0.05*
S. minor	9.68		0.27	0.61	0.25	0.21	0.65	0.94	0.41
S. minor	6.16	3.53		1.00	1.00	1.00	1.00	0.93	1.00
S. minor	6.97	2.71	0.82		1.00	1.00	1.00	1.00	1.00
P. escuilliei	6.07	3.62	0.09	0.91		1.00	1.00	0.92	1.00
P. escuilliei	5.95	3.73	0.20	1.02	0.11		1.00	0.89	1.00
D. rebouli	7.07	2.62	0.91	0.10	1.00	1.11		1.00	1.00
D. rebouli	7.94	1.74	1.78	0.97	1.88	1.99	0.87		0.98
Hyracoidea indet	6.52	3.16	0.37	0.45	0.46	0.57	0.54	1.42	

Paleocene mammals

Tukey's pairwise test Q / p (same)	PM40 *E. azzouzorum*	MNHN.F PM42 *E. azzouzorum*	PM100a *Eritherium*	PM66 *O. grandis*	MNHN.F PM39 *O. grandis*	PM101 *O. grandis*	MNHN.F PM54 *O. daouiensis*	MHNM.KHG.225 *Ocepeiidae?*	MHNM.KHG.226 *Ocepeiidae?*
E. azzouzorum		0.25	1.00	*< 0.05*	0.28	0.55	1.00	0.64	0.12
E. azzouzorum	3.70		0.63	*< 0.05*	1.00	*< 0.05*	0.36	1.00	*< 0.05*
Eritherium	1.03	2.67		*< 0.05*	0.68	0.20	1.00	0.96	*< 0.05*
O. grandis	5.78	9.48	6.81		*< 0.05*	0.53	*< 0.05*	*< 0.05*	0.98
O. grandis	3.59	0.10	2.56	9.37		*< 0.05*	0.40	1.00	*< 0.05*
O. grandis	2.86	6.56	3.90	2.92	6.46		0.40	*< 0.05*	0.98
O. daouiensis	0.36	3.33	0.67	6.15	3.23	3.23		0.78	0.08
Ocepeiidae?	2.66	1.04	1.63	8.44	0.94	5.52	2.29		0.00
Ocepeiidae?	4.32	8.02	5.35	1.46	7.92	1.46	4.69	6.98	

Supplementary Data Tables

SM Table 1 Supplementary trace element concentration and ratio data from Sidi Chennane and Sidi Daoui areas, focusing on some of the bone beds*:* the *Eritherium* bone bed (base Bed IIa), big coprolite bone bed (top Bed IIa), and *Otodus* bone bed (intercalary II/I). The Ce/Ce* and Pr/Pr*ratios are plotted in Figures 4 and 5 as a part of the background dataset.

SM Table 2 Major element compositions of marine remains (shark teeth, coprolites) from the Sidi Chennane quarry of the Ouled Abdoun Basin (see Figure 2 in the paper).

SM Table 3 Trace element concentrations, Ce/Ce* and Pr/Pr*ratios of the mammal specimens and related matrix from the Ouled Abdoun Basin investigated here (see Figures 3-5 in the paper).

SM Table 4 Student's t-tests on selected geochemical data displayed as boxplots in Figure 3. The six different types of materials studied are mammal enamel, dentine, bones, and shark tooth enameloid, dentine, and coprolites. Significant differences ($p < 0.05$) are marked red, whereas underlined data indicate unequal variances between the compared groups.

SM Table 5 Strontium isotope ratios of shark tooth enameloid from the Ouled Abdoun Basin (see Figure 7 in the paper). Individual analyses are plotted in Figure 7a, while the average data and derived Sr-isotope ages based on McArthur et al. (2020) are in Figure 7b.

SM Table 6 Ten defined chemostratigraphic horizons and their average Ce/Ce* values and the related F and Student's t-test statistics. df- degree of freedom; p- probability. Underlined p-values for the F-test indicate significantly different variances. In this case, the Student's t-tests were performed for unequal variance. The grey p-values for the Student's t-test highlights horizon pairs for which the means of the Ce/Ce* values do not differ significantly.

SM Table 7 Recovered selachian fauna and matrix data from a few mammal specimens belonging to the species *S. minor*, *S. major*, and *D. rebouli*.